AFRL-RH-WP-TR-2015-0084

IN VITRO STUDIES AND PRELIMINARY MATHEMATICAL MODEL FOR JET FUEL AND NOISE INDUCED AUDITORY IMPAIRMENT

Peter J. Robinson
Elaine A. Merrill
Andrea Hoffmann
Teresa R. Sterner
Henry M. Jackson Foundation
for the Advancement of Military Medicine
Wright-Patterson AFB OH

Mitchell L. Meade
David R. Mattie
Bioeffects Division
Molecular Bioeffects Branch

June 2015

Interim Report for April 2014 to September 2014

Molecular Bioeffects Branch
Bioeffects Division
Human Effectiveness Directorate
711th Human Performance Wing
Air Force Research Laboratory
Wright-Patterson AFB OH 45433-5707

NOTICE AND SIGNATURE PAGE

Using Government drawings, specifications, or other data included in this document for any purpose other than Government procurement does not in any way obligate the U.S. Government. The fact that the Government formulated or supplied the drawings, specifications, or other data does not license the holder or any other person or corporation; or convey any rights or permission to manufacture, use, or sell any patented invention that may relate to them.

Qualified requestors may obtain copies of this report from the Defense Technical Information Center (DTIC) (http://www.dtic.mil).

The experiments reported were conducted according to the "Guide for the Care and Use of Laboratory Animals," Institute of Laboratory Animal Resources, National Research Council.

(AFRL-RH-WP-TR - 2015 - 0084) has been reviewed and is approved for publication in accordance with assigned distribution statement.

MATTIE.DAVID.R.1230101880

Digitally signed by MATTIE.DAVID.R.1230101880
DN: c=US, o=U.S. Government, ou=DoD, ou=PKI, ou=USAF, cn=MATTIE.DAVID.R.1230101880
Date: 2016.01.07 15:55:58 -05'00'

DAVID R. MATTIE, Work Unit Manager
Molecular Bioeffects Branch

POLHAMUS.GARRETT.D.1175839484

Digitally signed by POLHAMUS.GARRETT.D.1175839484
DN: c=US, o=U.S. Government, ou=DoD, ou=PKI, ou=USAF, cn=POLHAMUS.GARRETT.D.1175839484
Date: 2016.01.21 08:17:10 -06'00'

GARRETT D. POLHAMUS, DR-IV, DAF
Chief, Bioeffects Division
Human Effectiveness Directorate
711th Human Performance Wing
Air Force Research Laboratory

This report is published in the interest of scientific and technical information exchange, and its publication does not constitute the Government’s approval or disapproval of its ideas or findings.

REPORT DOCUMENTATION PAGE

Form Approved
OMB No. 0704-0188

1. REPORT DATE *(DD-MM-YYYY)*	2. REPORT TYPE	3. DATES COVERED *(From - To)*
15-06-2015	Interim	April 2014 – September 2014

4. TITLE AND SUBTITLE

In Vitro Studies and Preliminary Mathematical Model for Jet Fuel and Noise Induced Auditory Impairment

5a. CONTRACT NUMBER
FA8650-10-2-6062

5b. GRANT NUMBER
NA

5c. PROGRAM ELEMENT NUMBER
62202F

6. AUTHOR(S)
Robinson, Peter J.[1]; Merrill, Elaine A.[1]; Hoffmann, Andrea[1]; Sterner, Teresa R.[1]; Qi, Lining[1]; Shiyanov, Pavel A.[1]; Mitchell L. Meade*; Mattie, David R.*

5d. PROJECT NUMBER
H0FS

5e. TASK NUMBER
30

5f. WORK UNIT NUMBER
03/H0FS

7. PERFORMING ORGANIZATION NAME(S) AND ADDRESS(ES)
[1]HJF, 2729 R St, Bldg 837, WPAFB OH 45433-5707

8. PERFORMING ORGANIZATION REPORT NUMBER

9. SPONSORING/MONITORING AGENCY NAME(S) AND ADDRESS(ES)
Air Force Materiel Command*
Molecular Bioeffects Branch
Bioeffects Division
Human Effectiveness Directorate
711th Human Performance Wing
Air Force Research Laboratory
Wright-Patterson AFB OH 45433-5707

10. SPONSOR/MONITOR'S ACRONYM(S)
711 HPW/RHDJ

11. SPONSORING/MONITORING AGENCY REPORT NUMBER
AFRL-RH-WP-TR-2015-0084

12. DISTRIBUTION AVAILABILITY STATEMENT
Distribution A. Approved for public release; distribution unlimited (PA Case No 88ABW-2016-0061, Date 7 Jan, 2016)

13. SUPPLEMENTARY NOTES

14. ABSTRACT
Laboratory studies in rats support the potential for jet fuel to promote noise induced hearing loss (NIHL). Occupational studies indicate that pilots, aircrew, and aircraft maintenance workers suffer higher rates of hearing loss. Jet fuel toxicity in association with noise may be at least partially explained by increased free radical production and oxidative stress at the cellular level. The project goal is to develop a multi-scale model to physiologically and mechanistically describe jet fuel exacerbated NIHL. This report describes the first five months of an ongoing effort. A pharmacodynamics (PD) model has been developed which describes the potential combined effect of jet fuel and noise on hearing loss via production of free radicals in cochlea hair cells. The PD model will be parameterized using results from in vitro studies. Initial proteomic studies with HEI-OC1 cells, a conditionally immortalized organ of Corti-derived epithelial cell line, indicate that JP-8 produces little cytotoxicity. Preliminary dose-response studies using the same cell type again revealed marginal cytotoxic effects when exposed to JP-8 or key hydrocarbons found in JP-8 and associated with chemically-induced hearing loss (toluene, ethylbenzene, xylene, nonane, or decane). However, apoptosis and necrosis were enhanced when cells were exposed to JP-8 or hydrocarbons with oligomycin (in vitro noise surrogate). The PD model is designed to interface with a physiologically-based pharmacokinetic (PBPK) model which will simulate delivery of JP-8 to the cochlea and other tissues during exposure.

15. SUBJECT TERMS
jet fuels, JP-8, hydrocarbons, hearing loss, noise, noise induced hearing loss, physiologically based pharmacokinetic model; PBPK, cochlea, in vitro

16. SECURITY CLASSIFICATION OF:			17. LIMITATION OF ABSTRACT	18. NUMBER OF PAGES	19a. NAME OF RESPONSIBLE PERSON
a. REPORT	b. ABSTRACT	c. THIS PAGE			D. R. Mattie
U	U	U	SAR	48	19b. TELEPONE NUMBER (*Include area code)* NA

Standard Form 298 (Rev. 8-98)
Prescribed by ANSI-Std Z39-18

THIS PAGE INTENTIONALLY LEFT BLANK.

TABLE OF CONTENTS

LIST OF FIGURES

LIST OF TABLES

THIS PAGE INTENTIONALLY LEFT BLANK.

PREFACE

Funding for this project was provided through the Air Force Office of Scientific Research (AFOSR) Laboratory Research Initiation Request (LRIR) 14RH09COR, under the program management of Pat Bradshaw, PhD (AFOSR/RTB). This research was conducted under contract FA8650-10-2-6062 with the Henry M. Jackson Foundation for the Advancement of Military Medicine (HJF). The program manager for the HJF contract was David R. Mattie, PhD (711 HPW/RHDJ), who was also the technical manager for this project.

The authors would like to acknowledge Frederico Kalinec at the David Geffen School of Medicine, University of California Los Angeles (UCLA), who kindly provided the House Ear Institute Organ of Corti 1 (HEI-OC1) cells.

THIS PAGE INTENTIONALLY LEFT BLANK.

1.0 SUMMARY

Laboratory studies in rats support the potential for jet fuel to promote noise induced hearing loss (NIHL). Occupational studies indicate that pilots, aircrew, and aircraft maintenance workers suffer higher rates of hearing loss. Jet fuel toxicity in association with noise may be at least partially explained by increased free radical production and oxidative stress at the cellular level. The goal of this project is to develop a multi-scale model to physiologically and mechanistically describe jet fuel exacerbated NIHL. This report describes accomplishments during the first five months of an ongoing effort.

A pharmacodynamic (PD) model has been developed which describes the potential combined effect of jet fuel and noise on hearing loss via the production of free radicals in the hair cells of the cochlea. The model assumes that free radical (FR) generation and oxidative stress combine to form the primary mechanism through which ototoxicants disrupt hearing and through which they potentiate the effects of noise on hearing loss. Inactivation of cellular targets, leading to hearing loss, is determined by the product of the steady-state FR concentration and the time of exposure of the target (cochlea) to that concentration. The model takes into account lipid peroxidation, and predicts additional biomarkers that can be measured (e.g., the oxidative stress marker malondialdehyde or glutathione depletion), as well as the loss of functionality (hearing loss) and hair cell death. The PD model will be parameterized using results from *in vitro* studies, and is designed to be interfaced with a physiologically-based pharmacokinetic (PBPK) model which will simulate the delivery of JP-8 to the cochlea and other tissues during exposure.

Initial proteomic studies with House Ear Institute Organ of Corti 1 (HEI-OC1) cells, a conditionally immortalized organ of Corti-derived epithelial cell line, indicate that JP-8 produces little cytotoxicity. At the highest dose of 500 ppm, proteomic changes primarily consist of upregulation of histones involved in chromatin remodeling as a result of oxidative stress. Although effects were not dramatic, a dose response was apparent.

Preliminary *in vitro* dose-response studies using the HEI-OC1 cells again revealed marginal cytotoxic effects when exposed to JP-8 or key hydrocarbons; these key hydrocarbons (toluene, ethylbenzene, xylene, nonane, or decane) are found in JP-8 and are also associated with chemically-induced hearing loss. Apoptosis and necrosis were enhanced when cells were exposed to JP-8 or hydrocarbons with oligomycin (an *in vitro* noise surrogate). Early induction of protective cellular mechanisms may explain the lack of cytotoxic effects at the two-hour time point. This is consistent with the upregulation of numerous histones.

2.0 INTRODUCTION

Laboratory studies support the potential for jet fuel to promote noise induced hearing loss (NIHL) (Fechter *et al.*, 2007, 2010, 2012; Guthrie *et al.*, 2014). Noise alone induces hearing loss due to loss of hair cells in the cochlea, associated with oxidative stress (Fechter, 2005; Henderson *et al.*, 2006; Poirier *et al.*, 2010). Jet fuel toxicity in association with noise may be at least partially explained by increased free radical production and oxidative stress at the cellular level (Boulares *et al.*, 2002), resulting in hair cell dysfunction and loss.

The ultimate goal of this project is to develop a multi-scale model to physiologically and mechanistically describe jet fuel exacerbated NIHL. To that end, the hypothesis can be stated as: Jet fuel exposure and noise exposure both produce oxidative stress in cochlear tissues, resulting in hearing loss when the oxidative stress exceeds glutathione reserves.

The project is arranged in three parts:

1. Develop a mathematical model to describe the impact of chemical and noise stressors at the target site (cochlea); free radical formation in the cochlea caused by chemical and/or noise stressors, lipid peroxidation, and free radical elimination by anti-oxidants; and the final impact on hair cell functionality and loss,

2. Design and implement *in vitro* experiments to measure oxidative stress and other markers of cytotoxicity in cochlea cells and to estimate values for key model parameters, and

3. Develop a pharmacokinetic model to describe the distribution of jet fuel components to the cochlea, in order to link jet fuel exposure and target site dosimetry with our pharmacodynamic (PD) model of oxidative stress and hearing loss.

This report describes the first five months of effort on this project.

2.1 Air Force Relevance

JP-8 is a kerosene-range jet fuel that is used by the U.S. Armed Services and North Atlantic Treaty Organization countries. JP-8 is the standard battle fuel for use in jets, vehicles, heaters, etc. in combat. The U.S. military alone consumes more than 2.5 billion gallons annually (Guthrie *et al.*, 2014).

Aircraft workers such as pilots, aircrew, aircraft technicians, and mechanics have high rates of hearing loss (32 to 47 percent prevalence) (Jaruchinda *et al.*, 2005) compared to normal adult populations (16.1 percent) (Agrawal *et al.*, 2008). Commercial aviation aircraft technicians and mechanics develop hearing loss at younger ages compared to age-matched individuals and to the general population (30 to 40 years old versus 60 to 69 years old, respectively) (Agrawal *et al.*, 2008). Air Force F-111 fuel tank maintenance workers have higher hearing thresholds compared to published data from otologically normal populations (Guest *et al.*, 2010); military fighter pilots and helicopter pilots are known to be at higher risk for developing hearing loss

(determined through audiometric assessments) compared to age-matched individuals in the general public (Agrawal *et al.*, 2008; Raynal *et al.*, 2006). This hearing loss occurs even with the use of hearing protections (Jaruchinda *et al.*, 2005).

Overexposure to noise is a key factor in the development of hearing loss. Measured noise levels of 91 to 110 dBA within the cockpit and around the aircraft may exceed the Occupational Safety and Health Administration (OSHA) permissible exposure limit (PEL) and the National Institute for Occupational Safety and Health (NIOSH) recommended exposure limit (REL) for the time period of exposure (Jaruchinda *et al.*, 2005). Preliminary epidemiologic data suggest that jet fuels (JP-4 or JP-8) may interact with noise to induce hearing loss (Kaufman *et al.*, 2005). Animal studies demonstrated that exposure to JP-8 combined with noise may result in the loss of preneural cochlear sensitivity, as shown by suppression of distortion product otoacoustic emissions (DPOAE) and depletion of cochlear sensory cells (Fechter *et al.*, 2007, 2010, 2012). The effect of combining the exposures (jet fuel plus noise) was greater than that of the individual exposures. Regulations regarding toxic exposures are generally based on exposure to a single agent; less is known about combined exposures such as jet fuel and noise.

2.2 Jet Fuel, Noise, and Hearing Loss

There is a growing body of laboratory studies supporting the potential for jet fuel to promote hearing loss when exposures include noise. Fechter *et al.* (2007) were the first to show that exposure to JP-8 followed by exposure to damaging noise resulted in decreased auditory function as well as cochlear outer hair cell loss in Long-Evans rats, compared to the effects of noise alone. Chemically enhanced hearing loss is generally accompanied by damage to outer hair cells of the cochlea. Researchers have hypothesized several specific mechanisms of toxicity to hair cells, including disruption of intracellular calcium homeostasis (Liu and Fechter, 1997), disruption of membrane fluidity (Campo *et al.*, 2001; Liu *et al.*, 1997), and disruption of efferent pathways synapsing at the cochlea (Lataye *et al.*, 2000). Free radical generation and oxidative stress as a possible pathway was investigated by Fechter (1999) and Rao and Fechter (2000). Fechter (2005) presented evidence that confirms the role of oxidative stress in the production of hearing loss by both carbon monoxide and by acrylonitrile when noise is present at the time of chemical exposure. Therefore, oxidative stress is a likely candidate for the role of jet fuel in mediating noise-induced hearing loss. This hypothesis is further supported by evidence that oxidative stress is linked to JP-8 exposure itself. Boulares *et al.* (2002) indicated that JP-8 toxicity might be at least partially explained by increasing oxidative stress at the cellular level; JP-8 reduced cellular glutathione (GSH) levels by approximately 40 percent in rat lung epithelial cells after only one hour of exposure.

Recent evidence suggests that central auditory processing dysfunctions (CAPD) are early manifestations of JP-8 induced ototoxicity. An experiment with Long-Evans rats (Guthrie *et al.*, 2014) showed that exposure to subtoxic levels of JP-8 (1000 mg/m^3) did not induce peripheral hearing loss. However, there was a CAPD that manifested as impaired brainstem encoding of stimulus intensity at four weeks after the exposure. Furthermore, this impairment in stimulus encoding was exacerbated by low level (non-damaging) noise (8 kHz octave band at 85 dB sound pressure level) exposure. The results revealed that subototoxic exposures to noise and JP-

8 resulted in normal peripheral auditory function concomitant with a CAPD. Thus it appears that CAPD may play a critical, and early, role in hearing loss in addition to oxidative stress-induced peripheral hair cell impairment and loss.

Altered growth functions of the brainstem components of the auditory brainstem response (ABR) are also characteristic of aging (Boettcher *et al.*, 1993; Popelar *et al.*, 2006; Zhou *et al.*, 2006). Potential mechanisms for such a process may include altered membrane fluidity (characteristic of solvent/anesthetic exposure) leading to potential impairments of vesicular transport and/or fusion at the synapses within the auditory brainstem. In humans, CAPD may be a first sign of subtle brain alteration (Bamiou *et al.*, 2000). Further, abnormal stimulus-response function in the central auditory nervous system has been associated with non-hearing disorders such as migraines and depression (Ambrosini *et al.*, 2003; Gallinat *et al.*, 2000). Oxidative stress may also play a role in CAPD (Henderson *et al.*, 2006).

In addition, postulated mechanisms for tinnitus show an interesting connection between loss of peripheral cells and compensatory mechanisms in the rest of the auditory pathway (Schaette and Kempter, 2012). Lateral inhibition is ubiquitous in the brain, and it is assumed to be a basic mechanism of information processing in neural circuits. In the auditory pathway, inhibition exists between frequency channels, i.e., inhibition between neurons whose characteristic frequency is close, but not identical. These frequency channels are associated with specific hair cells, and as specific hair cells become inactive, inhibition of neighboring (and still functional) pathways becomes dis-inhibited, which could amplify differences in spontaneous activity. Mathematical models of this activity have been developed (e.g., Schaette and Kempter, 2012).

3.0 MATHEMATICAL MODEL OF FREE RADICAL MEDIATED HEARING LOSS

For the current project, the working hypothesis is that free radical (FR) generation and oxidative stress combine to form the primary mechanism through which ototoxicants disrupt hearing and through which they potentiate the effects of noise on hearing loss. This hypothetical working relationship is outlined in Figure 1. A previous technical report (Robinson *et al.*, 2013) provided an outline for combining models for dosimetric predictions of JP-8 at the target site (via a physiologically-based pharmacokinetic (PBPK) model), together with its effect, and the effect of noise, on the generation of free radicals in the cochlea, and their impact on inducing cellular damage and hearing loss. That model was based on an earlier model (Byczkowski *et al.*, 1997) that described the removal of FRs in terms of a lumped rate constant for FR recombination and quenching. The model assumed that the inactivation of cellular targets, leading to hearing loss, was determined by the product of the steady-state FR concentration and the time of exposure of the target (cochlea) to that concentration.

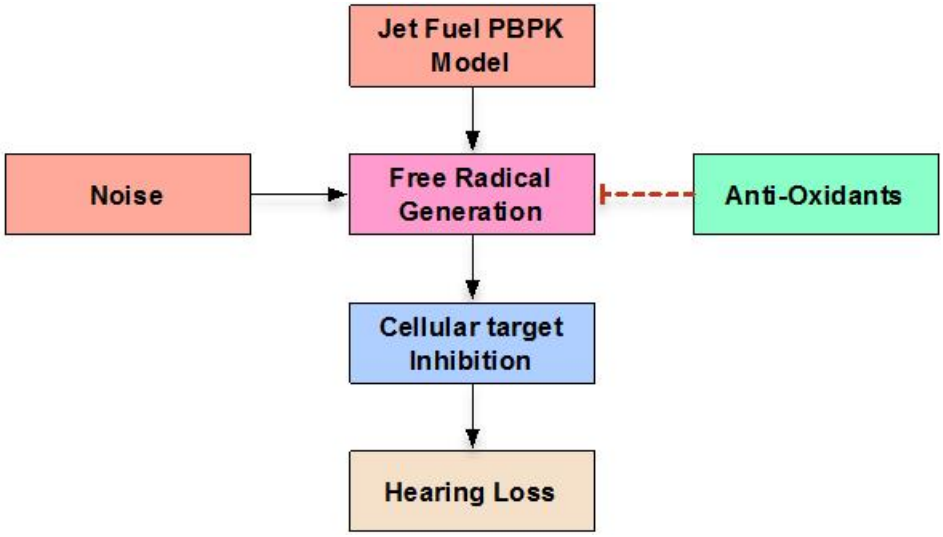

Figure 1. Schematic of Overall Scope of Project

The operational equations for chemical mixture plus noise - induced free radical generation were derived as:

$$\frac{dFR}{dt} = \sum_{i=1,m} k_i C_i + k_N N + \sum_{i=1,m} k_{xi} C_i.N - k_t FR \quad (1)$$

…, which in the steady-state (dFR/dt = 0), becomes:

$$FR = \left(\sum_{i+1,m} k_i C_i + k_N N + \sum_{i=1,m} k_{xi} C_i.N\right)/k_t \quad (2)$$

…, where C_i is the local (cochlear) pro-oxidant concentration of chemical i, k_i is the rate constant of free radical formation from the pro-oxidant chemical (1/hour), N is local (cochlear) nose intensity level, k_N is a rate constant of free radical formation from the noise (1/hour), and k_t is the lumped rate constant of free radical recombination and quenching by the biological system (1/hour). In order to take into account the likely synergism between each chemical and noise in local free radical production at the cochlea, an interaction term is introduced as a cross-product ($k_{xi}C_i.N$).

The activity of hair cells, reduced by FR-induced inactivation, was given as:

$$I_n = I_0 \, exp\left(-k_d.FR.t_p\right) \quad (3)$$

…, where k_d is the rate constant for cellular target inactivation by free radicals, I_n is remaining activity, expressed as a fraction of remaining active cellular targets, relative to the amount before inhibition; I_0 is initial concentration of active cellular targets (assumed 100 percent); and t_p is time of exposure to free radicals at local steady state concentrations.

Finally, combining equations (2) and (3), we have that the fractional hearing functionality remaining f_n is given by:

$$f_n = \frac{I_n}{I_0} = \exp - \left(\frac{\left(\sum_{i=1,m} k_i C_i + k_N N + \sum_{i=1,m} k_{xi} C_i . N \right) k_d t_p}{k_t} \right) \quad (4)$$

The objective of the current project is to further develop this preliminary model so as to also take into account the following:

- The time-course, not just the steady-state concentrations, of FRs in the cochlea, so that the inactivation of the target sites is dependent on a more dynamic "area under the FR concentration-time curve" calculation, rather than simply proportional to the steady-state concentration of free radicals multiplied by some estimate of the "time of exposure" to this concentration,
- Lipid peroxidation (the generation of lipid peroxides, such as polyunsaturated fatty acid radicals (PUFAR) and peroxy polyunsaturated fatty acid radicals (PPUFAR)),
- Linkage of the model to additional biomarkers that can be measured (e.g., the oxidative stress marker malondialdehyde or glutathione depletion), and
- The loss of functionality (hearing loss) and hair cell death.

At this stage in model development, jet fuel and noise are being described as a single "lumped" stressor. Cross-terms reflecting synergy between noise and chemicals have not yet been added.

3.1 Model Description

Figure 2 shows a schematic of the current model. Hair cells in the cochlea are exposed to chemical at a concentration C1 (via the circulation) and/or noise (of intensity N). Free radicals are produced by stressors; they are reduced by GSH and other anti-oxidants (represented by GSH in Figure 2). FRs also interact with lipid membranes (represented by polyunsaturated fatty acids (PUFA)), producing PUFAR and PPUFAR in a cascading process that also produces lipid peroxides (LP) and malondialdehyde (MDA). MDA is a thiobarbituric acid reactive substance (TBARS) quantified by the TBARS assay.

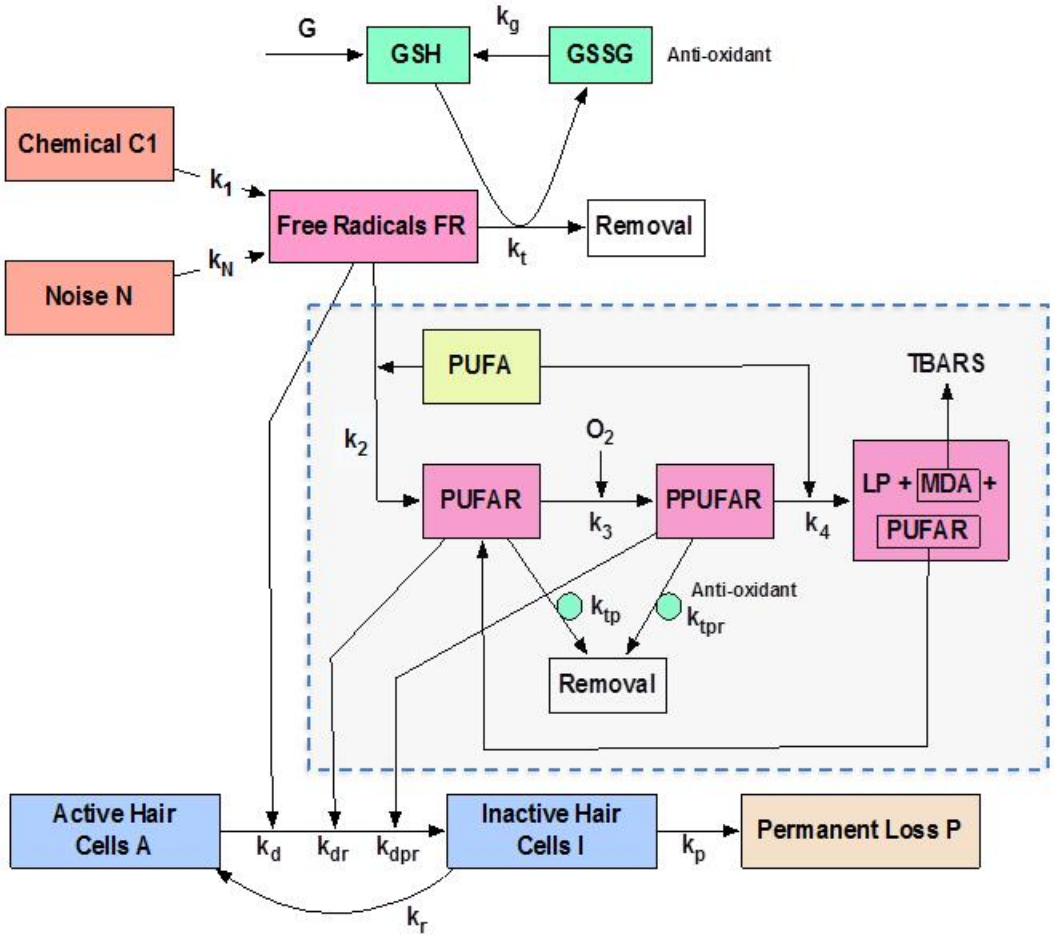

Figure 2. Schematic for Chemical- and Noise-Induced Hair Cell Inactivation and Death as a Result of Free Radical Generation in the Cochlea. FR: free radical; GSH: glutathione; k variables: rate constants; PUFA: polyunsaturated fatty acids; PUFAR: polyunsaturated fatty acid radicals; PPUFAR: peroxyl polyunsaturated fatty acid radicals; LP: lipid peroxides; MDA: malondialdehyde; TBARS: thiobarbituric acid reactive substance

For a single chemical (i=1), and with no interaction term between chemical and noise, equation (1) for the free radical concentration reduces to:

$$\frac{dFR}{dt} = k_1 C_1 + k_N N - k_t FR \tag{5}$$

…, where k_1 and k_N are rate constants for FR production by the chemical and noise, respectively, and k_t is the degradation rate constant for FR.

Glutathione (and the inactivated glutathione disulfide, GSSG) concentrations are given by:

$$\frac{dGSH}{dt} = G + k_g GSSG - k_t GSH.FR - k_{tp} GSH.PUFAR - k_{tpr} GSH.PPUFAR \tag{6}$$

$$\frac{dGSSG}{dt} = -k_g GSSG + k_t GSH.FR + k_{tp} GSH.PUFAR + k_{tpr} GSH.PPUFAR \quad (7)$$

…, where k_t, k_{tp}, and k_{tpr} are rate constants for the oxidation of GSH by FR, PUFAR, and PPUFAR respectively, k_g is the rate constant for the recycling of GSSG, and G is the GSH synthesis rate.

Polyunsaturated fatty acid radical concentrations are given by:

$$\frac{dPUFAR}{dt} = k_2 FR.PUFA - k_3 O_2.PUFAR + k_4 PUFAR.PUFA - k_{tp} PUFAR.GSH \quad (8)$$

…, where k_2 and k_4 are rate constants for polyunsaturated fatty acid oxidation by FR and other polyunsaturated fatty acid radicals, and k_3 is a rate constant for conversion of PUFAR into PPUFAR in the presence of oxygen at concentration O_2.

Peroxy-polyunsaturated fatty acid radical concentrations in turn are given by:

$$\frac{dPPUFAR}{dt} = k_3 O_2.PUFAR - k_4 PUFAR.PUFA - k_{tpr} PPUFAR.GSH \quad (9)$$

Active (A), inactive (I), and permanently damaged (P) hair cell concentrations are given by:

$$\frac{dA}{dt} = -k_d FR + k_r I - k_{dr} PUFAR - k_{dpr} PPUFAR \quad (10)$$

$$\frac{dI}{dt} = k_d FR - k_r I - k_p I + k_{dr} PUFAR + k_{dpr} PPUFAR \quad (11)$$

$$\frac{dP}{dt} = k_p I \quad (12)$$

…, where k_d, k_{dr}, and k_{dpr} are rate constants for the inactivation of hair cells by FR, PUFAR, and PPUFAR, respectively; k_r is the rate constant for repair of inactive cells, and k_p for the conversion of inactive, but repairable cells, into permanently damaged and inactive cells (cell death).

The model was implemented in Berkeley Madonna (Macey and Oster, University of California, Berkeley CA). The model code is given in the Appendix.

3.2 Model Simulations

Figure 3 shows time-course predictions of the model under separate and combined chemical and noise exposures, for FR, PUFAR, PPUFAR, GSH, and its oxidized form GSSG levels.

Parameter values are arbitrary at this point but the model simulations show the expected behavior of the model structure. The figure panels also show predicted levels of MDA, a substrate for the TBARS assay. In addition, the fraction of hair cells *A* that remain active is also shown. Note the partial recovery of active hair cells when either chemical or noise exposure is removed (Figures 3A and B). Note that in this particular simulation, chemical and noise stressors reduce the final active hair cells *A* by about 6.6 percent and 7.8 percent, respectively, whereas the combination reduces *A* by about 15.8 percent (Figure 3C). Figure 3D shows the effect of introducing a cross term (kx1 = 10, expressing hypothetical synergy between noise and chemical), which further reduces the final number of active cells, in this case by about 30 percent.

3.3 Conclusion

The current model describes the potential combined effect of jet fuel and noise on hearing loss via the production of free radicals in the hair cells of the cochlea. It can be integrated with PBPK models of jet fuel components (in both experimental animals and humans), as well as information about noise exposure, to predict hearing loss via this specific mechanism. The limitations of the present model, and potential improvements, are discussed in Section 4.1 below.

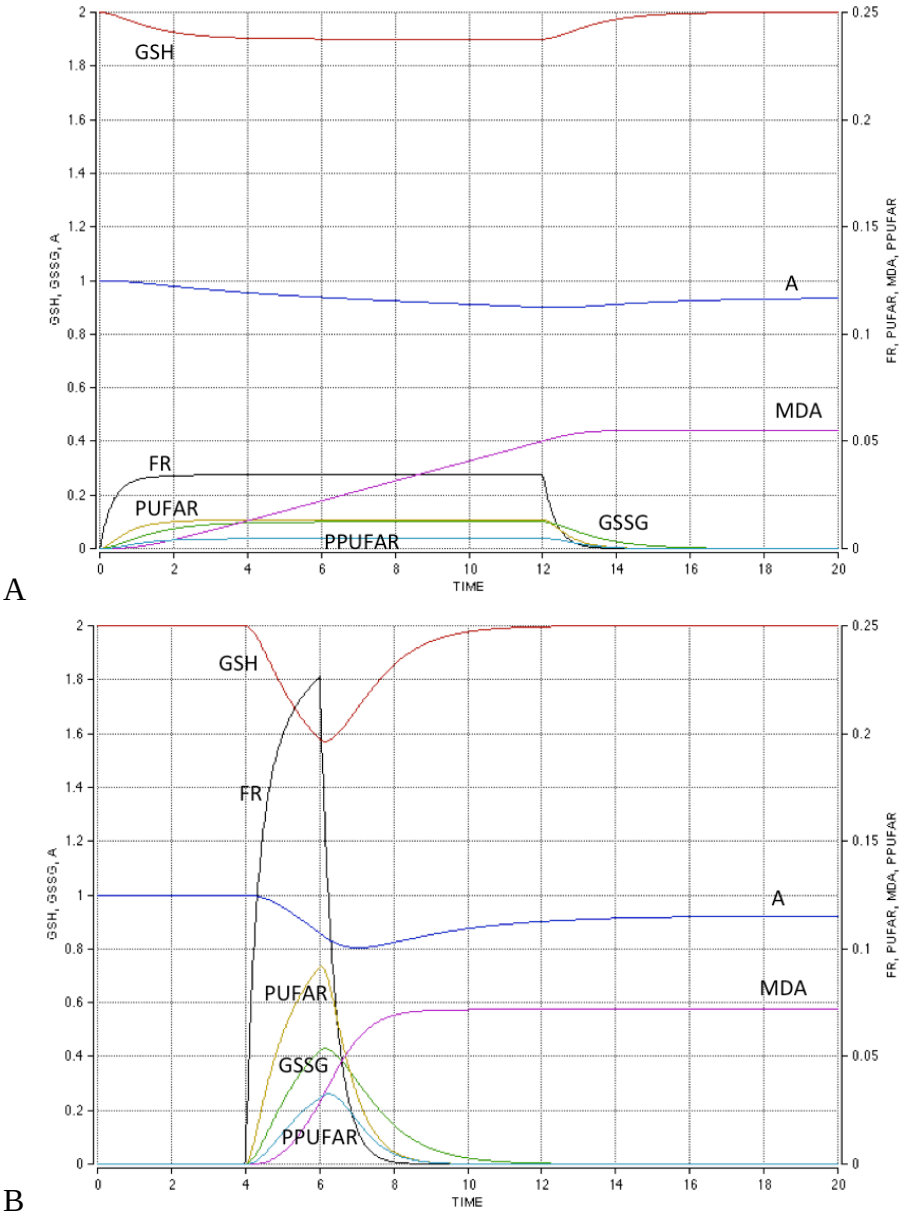

Figure 3. Representative Model Simulations showing the Response of the System to Chemical and/or Noise Exposure. Plots show chemical concentration (C) = 0.1 units (Panel A) for 12 hours, or a pulse of noise N = 0.6 units (Panel B) from time t = 4 to t = 6. Panel C (next page) shows the combined effect of both noise and chemical. Panel D shows the effect of introducing a cross term (kx1 = 10) expressing hypothetical synergy between noise and chemical. *A*: fraction of active hair cells; FR: free radical levels; GSH: glutathione; GSSG: glutathione disulfide; MDA: malondialdehyde; PUFAR: polyunsaturated fatty acid radicals; PPUFAR: peroxy polyunsaturated fatty acid radicals

C

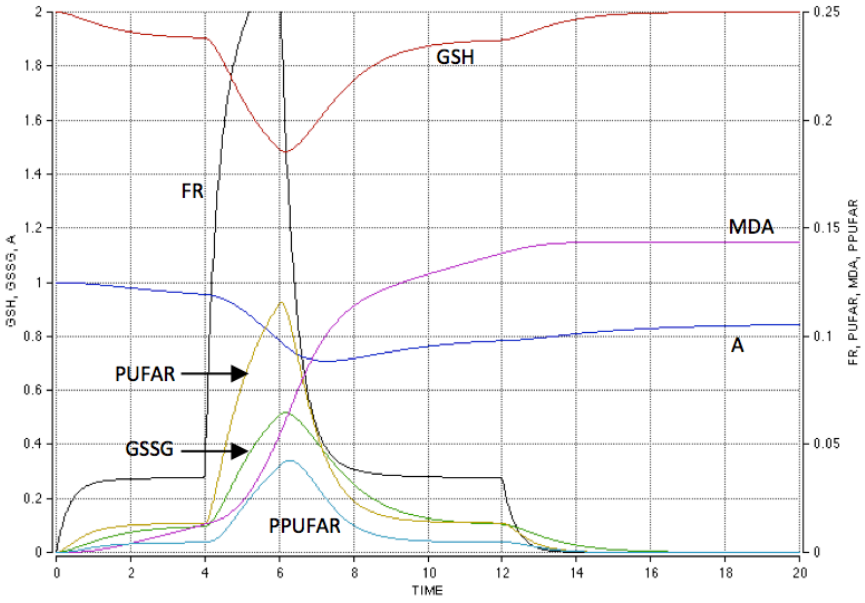

D

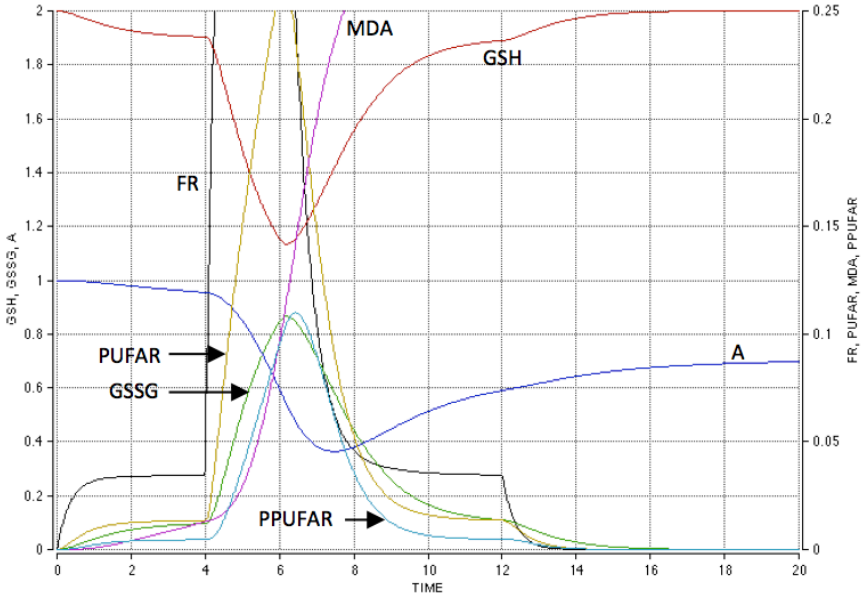

Figure 3 (continued). Panel C shows the combined effect of both noise and chemical. Panel D shows the effect of introducing a cross term (kx1 = 10) expressing hypothetical synergy between noise and chemical. *A*: fraction of active hair cells; FR: free radical levels; GSH: glutathione; GSSG: glutathione disulfide; MDA: malondialdehyde; PUFAR: polyunsaturated fatty acid radicals; PPUFAR: peroxy polyunsaturated fatty acid radicals

4.0 *IN VITRO* STUDIES

4.1 Introduction

A number of *in vitro* methods were proposed to explore the effect of JP-8, key hydrocarbons, and a noise surrogate (oligomycin) on cellular function and viability. Two studies, a 24-hour proteomic study of House Ear Institute Organ of Corti 1 (HEI-OC1) cells exposed to JP-8 (Section 4.2), and a study of the effects of JP-8 and five key components on apoptosis and necrosis in HEI-01 cells (Section 4.3), were completed. Other studies to monitor oxidative stress (to include other cell types) and extend the studies to the cells of the auditory brainstem are planned (see Section 5.2 below).

The time course of GSH depletion and other measures of oxidative stress in cochlea are unknown. Potentially novel biomarkers of oxidative stress and lipid peroxidation can be identified using a proteomic approach (Section 4.2). GSH depletion is measureable *in vitro* using a conditionally immortalized organ of Corti-derived epithelial cell line, which shows evidence of activation of apoptosis when exposed to known ototoxic chemicals (Kalinec *et al.*, 2003). This cell line is a recently developed *in vitro* system to investigate the cellular and molecular mechanisms involved in ototoxicity, and for screening of the potential ototoxic properties of jet fuel components and other chemical stressors.

Monitoring GSH levels and GSH depletion rates provides critical information regarding the cellular ability to protect against oxidative damage. In a single step experiment using a GSH specific fluorophore (Thiol Green Indicator, AbCam, Cambridge MA), the levels of GSH and GSSG can be obtained in a high-throughput manner using a fluorescence assay. This method provides single-point GSH levels and GSH/GSSG ratios that are observed over a time-course of JP-8 exposure, resulting in a kinetic profile of JP-8 effect on oxidative resistance capacity.

Further information regarding the oxidative stress levels within live cells can be obtained using fluorescent dyes specific for cytosolic ROS (CellROX Deep Red Reagent, Invitrogen, Carlsbad CA) and for mitochondrial superoxide (MitoSOX Red Indicator, Invitrogen). These parameters are highly indicative of the health of a given cell; oxidative stress in the mitochondria is directly related to onset of cellular death. By using live cell compatible dyes, microscopic images are achieved real-time during the JP-8 exposure. This experimental method provides ROS production rates that are otherwise unobtainable.

Finally, the levels of oxidative stressors within the cell need to be related to cellular death and cytotoxicity of JP-8 exposure (Section 4.3). Cytotoxicity can be measured by a simple, single step absorbance based assay based upon the formation of a soluble formazan product indicating the number of live cells in a culture (CellTiter 96 AQueous One Solution Cell Proliferation Assay, Promega Corporation, Madison WI). By correlating JP-8 exposure, ROS production, GSH depletion, and cytotoxicity, a full picture of the JP-8 effect on cochlear cells may be obtained, and these parameters can be used in developing a multi-scale model.

4.2 Proteomic Pathway Analysis of 24-Hour JP-8 Exposure using a Cochlear Cell Model and Cellular Pathway Modulation

The purpose of this study was to identify potentially novel biomarkers of JP-8 toxicity in a cochlear cell line using a proteomic approach. Biomarkers of oxidative stress and lipid peroxidation were investigated.

4.2.1 Cell Culture and Exposure Methods. Conditionally immortalized HEI-OC1 auditory cells isolated from the Organ of Corti were provided by Federico Kalinec, PhD (David Geffen School of Medicine, Department of Head and Neck Surgery, University of California, Los Angeles CA). The development and characterization of these cells is described in Kalinec *et al.* (2003).

The cells were cultured in Cellstar® T-25 cell culture flasks (Greiner Bio-One, Monroe NC) in high glucose Dulbecco's modified Eagle's medium (DMEM), supplemented with 10 percent fetal bovine serum at 33˚C under 5 percent CO_2 in an incubator. At approximately 80 percent confluence, media was removed, and flasks (60 ml) were filled, leaving no head space, with complete culture medium containing concentrations of 0, 0.5, 5, 50, or 500 ppm JP-8 jet fuel. Plug-seal caps were tightly installed to prevent loss of volatiles. These conditions may result in oxygen deprivation and lower pH. However, at 24 hours of exposure, cell cultures were examined by phase-contrast microscopy, and no visible signs of cell death were seen across all concentrations, including controls. Media was then removed, and cells were harvested by scraping and rinsing the flask with phosphate buffered saline (PBS). Cells were pelleted by centrifugation at 100 G for 5 minutes and PBS was removed.

4.2.2 Tandem Mass Tags (TMT) Liquid Chromatography-Tandem Mass Spectrometry (LC-MS/MS). Approximately $1x10^6$ cells were placed in 100 µL of lysis buffer (8 M urea, 50 mM triethyl ammonium bicarbonate (TEAB), 75 mM NaCl), and homogenized with a handheld pestle homogenizer. Protein samples were further processed by addition of 5 mM tris (2-carboxylethyl) phosphine hydrochloride (TCEP) and 15 mM iodoacetamide for reduction and alkylation of cysteines. Small aliquots of each sample were taken to perform protein concentration using the Bradford assay from Bio-Rad (Hercules CA). The remaining samples were diluted and digested overnight at 37°C with 4 µg of trypsin, followed by quenching with 1 percent formic acid. Samples were desalted using a C18 peptide trap from Michrom (Auburn CA). The desalted samples were vacufuged and processed by TMT labeling according to the manufacturers' instructions (Applied Biosystems, Life Technologies, Grand Island NY). Samples were labeled with the mass/charge TMT tag scheme of 126, 128, 129, 130, and 131, referring to 0, 0.5, 5, 50, and 500 ppm JP-8 jet fuel exposures, respectively. The TMT labeled samples were combined, the fluid volume was brought up to 100 µL with 0.1 percent formic acid in water, and the resulting sample placed in the auto-sampler for injection.

Peptides were separated on a Waters BEH C18 capillary column (Milford MA) prior to online analysis using a 240-minute increasing gradient of acetonitrile with 0.1 percent formic acid. Following elution from the column, ions were generated using 1.4 kV on a coated capillary tip in

a New Objective source and entered into the linear trap quadripole (LTQ)-Orbitrap Velos MS (Thermo Fisher, San Jose CA). In the MS, a full scan was taken in the LTQ, followed by data-dependent MS/MS analysis of the top eight peaks. MS/MS analysis included collision-induced dissociation in the LTQ for structural information and higher-energy collisional dissociation in the Orbitrap for quantitation. To enable low abundance detection, peptide analysis was executed under dynamic exclusion, followed by peptide alignment with a mammalian protein database using the SEQUEST algorithm in Proteome Discoverer 1.3 (Thermo Fisher, San Jose CA). Variable modifications for TMT oxidation at the N-terminus, oxidation at M-terminus, and carboxymethylation at the C-terminus were included in the database search. TMT ratios were calculated by normalization against the control.

4.2.3 Computational Gene Ontology Analysis. SEQUEST defined UniProt/SwissProt accession numbers were converted via the identification (ID) mapping tool of the UniProt webpage (http://www.uniprot.org) into Ensembl Protein IDs that were then converted via the BioMart Portal (central.biomart.org) into WikiGenes names (http://www.wikigenes.org). The WikiGenes names of all regulated proteins were entered into Cytoscape 3.1.1. through the ClueGo 2.1.3 application in two sets: 1) above 1.2-fold expression (upregulated), and 2) below 0.83-fold expression (downregulated) for gene ontology (GO) analysis including searches for GO biological process, GO cellular component, GO molecular function, GO immune system process, Kyoto Encyclopedia of Genes and Genomes (KEGG) PATHWAY database (Kyoto University, Kyoto, Japan), Reactome, and Wiki pathway at medium to detailed network specificity setting.

4.2.4 Results. The TMT MS relative peptide quantitation of HEI-OC1 cells tissue defined 994 UniProt/SwissProt identifiers (European Bioinformatics Institute, Cambridge UK) using SEQUEST software of which 9.55 percent were upregulated in expression (above 1.2 fold) and 4.42 percent were downregulated (below 0.83 fold) following various JP-8 exposure levels (0.5 to 500 ppm) compared to the naïve control (Table 1). SEQUEST defined UniProt/SwissProt accession numbers that were converted via the ID mapping tool of the UniProt webpage (http://www.uniprot.org) into Ensembl Protein IDs, which resulted in 1006 identified Wiki Gene names when further converted via the BioMart Portal (central.biomart.org). Due to multiple Ensemble Protein IDs for the same WikiGene name, 368 valid entries were found when entered into Cytoscape 3.1.1. Of these only 20 nodes were downregulated below 0.83-fold and 47 were upregulated above 1.2-fold.

The ClueGo analysis of WikiGenes identifiers for modulated proteins was able to define GO terms for 97.87 to 100 percent of the entered query. In detail, GO term analysis of modulated proteins following JP-8 exposure was limited to an upregulation of histones belonging to the histone subfamilies HIST1H, HIST2H, and HIST4H that regulate chromatin remodeling in response to oxidative cell stress, gene expression, cell cycle progression, cell differentiation through Wnt signaling, cell inflammation through interferon gamma signaling, and cell senescence (Figures 4 and 5). Under the ClueGO analysis, proteins important for energy regulation such as oxoglutarate dehydrogenase, were upregulated approximately 1.2-fold following 50 to 500 ppm JP-8 (Table 1). In addition, enolase (ENO1), a marker for

neuroinflammatory processes, was upregulated at higher doses of 50 to 500 ppm to approximately 1.7 to 1.4-fold. As a sign of JP-8 dependent activation of cell signaling, the protein kinase A-associated protein (AKAP) and the inositol trisphosphate receptor (ITPR2) were upregulated approximately 1.2-fold. The palmitoyl transferase (SPTLC3) that is involved in ceramide synthesis was upregulated at all doses, suggesting impact of JP-8 on membrane-structural components.

Proteins downregulated following JP-8 were classified by GO terms for cytochrome oxidase metabolism, microglia differentiation, RNA expression, and adenosine triphosphate (ATP) transport (Figures 6 and 7). In detail, proteins that were downregulated included the DNA damage sensor kinase (ATR), which was downregulated to approximately 0.6 to 0.77-fold at doses between 5 to 500 ppm JP-8. The reactive oxygen quencher and energy regulator, cytochrome oxidase 10, and the ATP transporter, SLC25A4, were downregulated to approximately 0.82-fold at the highest concentration of JP-8, suggesting that JP-8 has a toxic impact at higher doses. Among the ClueGO non-recognized downregulated proteins were proteins important for structural integrity including microtubule-associated protein (MAP1) that decreased at doses between 5 to 500 ppm JP-8 and S100A6 that decreased at the highest dose to 0.63-fold (Table 1).

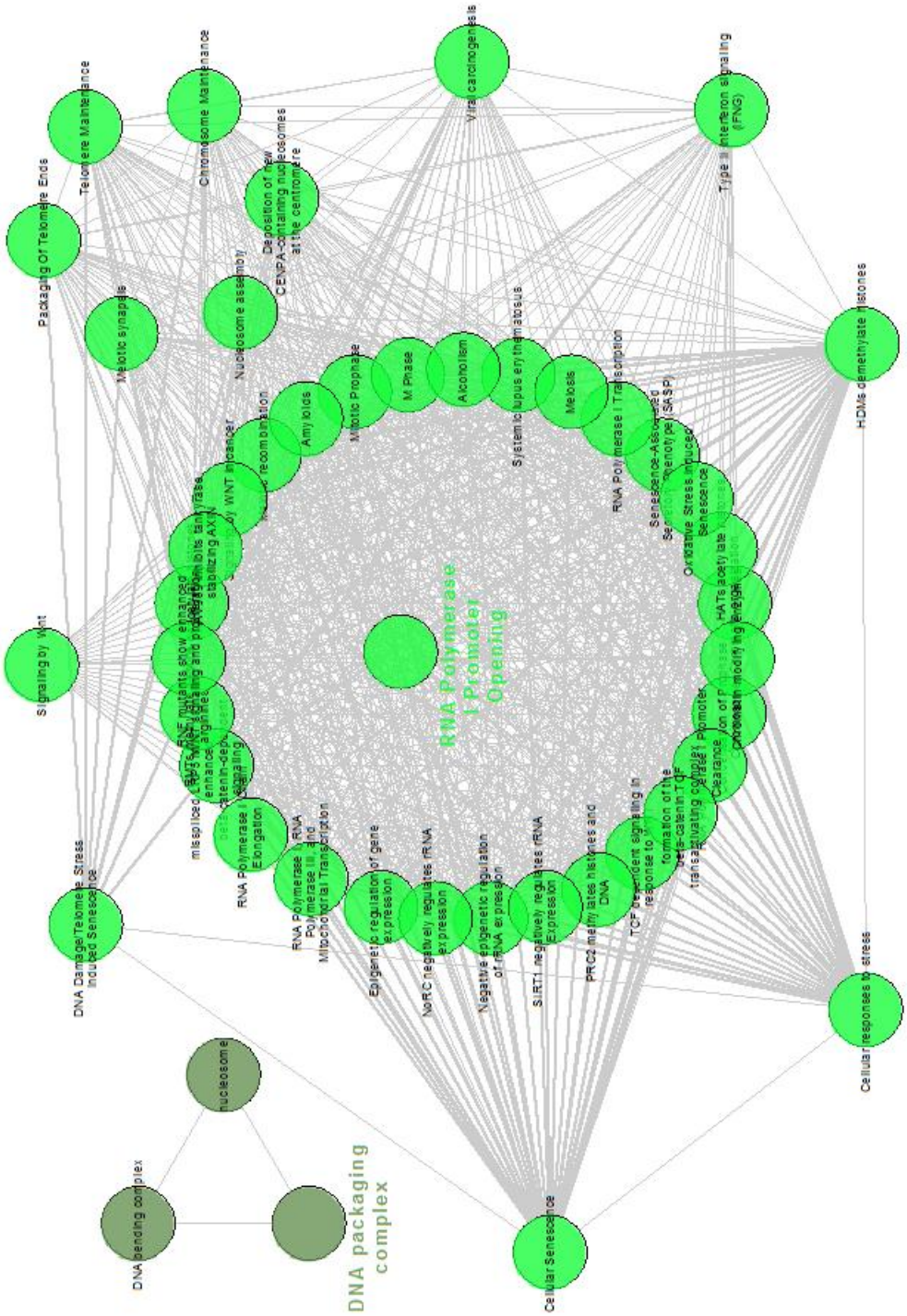

Figure 4. GO Term Pathway Analysis of Upregulated Proteins following JP-8 Exposure

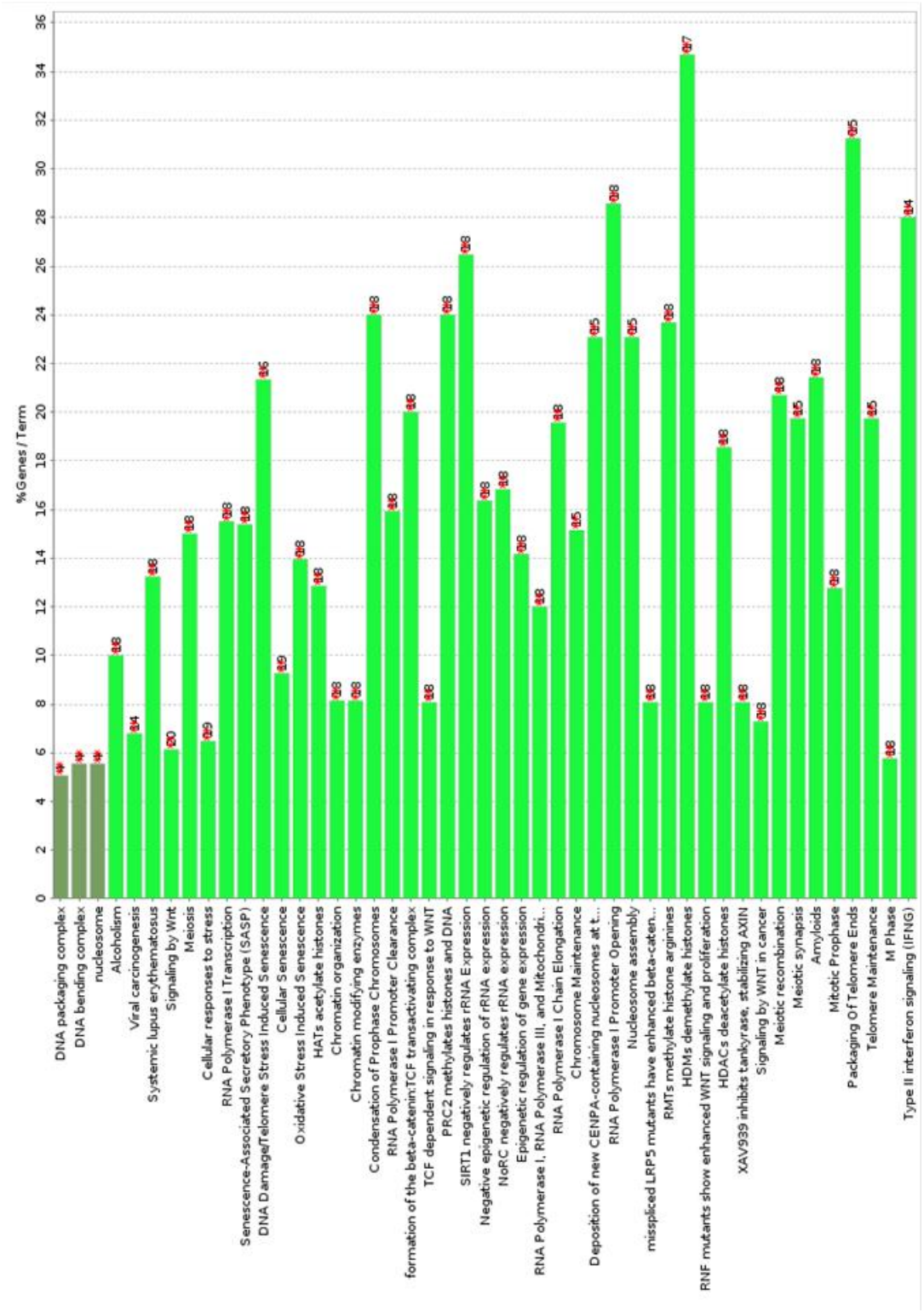

Figure 5. GO Term Bar Chart Analysis of Upregulated Proteins following JP-8 Exposure

Table 1. List of JP-8 Modulated Proteins in HEI-OC1 Cells

Description	Ensembl Protein ID	swiss prot accesssion	0.5 ppm	5 ppm	50 ppm	500 ppm	Wiki-Genename
A kinase (PRKA) anchor protein 13, isoform CRA_a OS=Homo sapiens GN=AKAP13 PE=1 SV=2 - [A8MYJ1_HUMAN]	ENSP00000378018	A8MYJ1	1.12785601	1.130950191	1.199149462	1.208043468	AKAP13
Isoform 2 of Probable phospholipid-transporting ATPase IIB OS=Homo sapiens GN=ATP9B - [ATP9B_HUMAN]	ENSP00000304500	O43861-2	1.117123661	1.072520368	1.209841183	1.083888924	ATP9B
Serine/threonine-protein kinase ATR OS=Homo sapiens GN=ATR PE=1 SV=3 - [ATR_HUMAN]	ENSP00000372581	Q13535	0.865087904	0.60016932	0.781477307	0.774224269	ATR
Isoform 2 of Transcription factor BTF3 OS=Homo sapiens GN=BTF3 - [BTF3_HUMAN]	ENSP00000338516	P20290-2	1.24625958	1.163113429	1.158156833	1.11743222	BTF3
Uncharacterized protein C12orf55 OS=Homo sapiens GN=C12orf55 PE=4 SV=4 - [E9PJL5_HUMAN]	ENSP00000431759	E9PJL5	1.513583318	0.929137772	1.20967811	1.195255884	C12orf63
Uncharacterized protein C1orf141 OS=Homo sapiens GN=C1orf141 PE=2 SV=1 - [CA141_HUMAN]	ENSP00000444018	Q5JVX7	0.829047291	1.027215651	0.854879766	0.935728278	C1orf141
Coiled-coil domain-containing protein 136 (Fragment) OS=Homo sapiens GN=CCDC136 PE=4 SV=1 - [H0Y876_HUMAN]	ENSP00000417991	H0Y876	0.795248992	0.775623845	0.952952735	1.092386402	CCDC136
Coiled-coil domain-containing protein 168 OS=Homo sapiens GN=CCDC168 PE=2 SV=2 - [CC168_HUMAN]	ENSP00000320232	Q8NDH2	1.075755467	1.145834788	1.218241177	1.202870667	CCDC168
Isoform 2 of T-complex protein 1 subunit zeta-2 OS=Homo sapiens GN=CCT6B - [TCPW_HUMAN]	ENSP00000400917	Q92526-2	0.93895319	0.768856583	0.6992221	0.963421384	CCT6B
Protoheme IX farnesyltransferase, mitochondrial OS=Homo sapiens GN=COX10 PE=2 SV=1 - [B4DFR1_HUMAN]	ENSP00000443354	B4DFR1	0.906783539	0.854203986	0.89138518	0.82704451	COX10
Isoform 3 of Dynactin subunit 1 OS=Homo sapiens GN=DCTN1 - [DCTN1_HUMAN]	ENSP00000386406	Q14203-3	1.217055639	1.097390165	0.953469148	1.16562763	DCTN1
dCTP pyrophosphatase 1 OS=Homo sapiens GN=DCTPP1 PE=1 SV=1 - [DCTP1_HUMAN]	ENSP00000322524	Q9H773	0.975338746	0.823766018	0.838201163	0.995544648	DCTPP1
Dynein heavy chain 10, axonemal OS=Homo sapiens GN=DNAH10 PE=1 SV=4 - [DYH10_HUMAN]	ENSP00000386770	Q8IVF4	0.861600789	0.763915905	0.772915068	0.887358245	DNAH10
Protein downstream neighbor of Son (Fragment) OS=Homo sapiens GN=DONSON PE=4 SV=1 - [H7C1M7_HUMAN]	ENSP00000401082	H7C1M7	0.960208804	1.256592052	1.326815667	1.206947936	DONSON
Protein dpy-30 homolog OS=Homo sapiens GN=DPY30 PE=1 SV=1 - [DPY30_HUMAN]	ENSP00000345837	Q9C005	0.947382945	0.914421945	0.786640025	0.935408805	DPY30
Alpha-enolase OS=Homo sapiens GN=ENO1 PE=1 SV=2 - [ENOA_HUMAN]	ENSP00000234590	P06733	1.113900924	1.122672924	1.709191186	1.431079916	ENO1
Gem-associated protein 4 OS=Homo sapiens GN=GEMIN4 PE=1 SV=2 - [GEMI4_HUMAN]	ENSP00000321706	P57678	1.050920216	0.850676387	1.489901748	1.366101953	GEMIN4
Histone H1.5 OS=Homo sapiens GN=HIST1H1B PE=1 SV=3 - [H15_HUMAN]	ENSP00000330074	P16401	1.433721943	1.496346219	1.577065064	1.468242521	HIST1H1B
Histone H2A type 1-C OS=Homo sapiens GN=HIST1H2AC PE=1 SV=3 - [H2A1C_HUMAN]	ENSP00000473534	Q93077	1.097503285	1.14628214	1.311780458	1.00192943	HIST1H2AC
Histone H4 OS=Homo sapiens GN=HIST1H4A PE=1 SV=2 - [H4_HUMAN]	ENSP00000476824	P62805	1.784160043	1.960381758	2.172168563	2.323679014	HIST1H4A
Histone H4 OS=Homo sapiens GN=HIST1H4A PE=1 SV=2 - [H4_HUMAN]	ENSP00000476824	P62805	1.784160043	1.960381758	2.172168563	2.323679014	HIST1H4B
Histone H4 OS=Homo sapiens GN=HIST1H4A PE=1 SV=2 - [H4_HUMAN]	ENSP00000476824	P62805	1.784160043	1.960381758	2.172168563	2.323679014	HIST1H4C
Histone H4 OS=Homo sapiens GN=HIST1H4A PE=1 SV=2 - [H4_HUMAN]	ENSP00000476824	P62805	1.784160043	1.960381758	2.172168563	2.323679014	HIST1H4D
Histone H4 OS=Homo sapiens GN=HIST1H4A PE=1 SV=2 - [H4_HUMAN]	ENSP00000476824	P62805	1.784160043	1.960381758	2.172168563	2.323679014	HIST1H4E
Histone H4 OS=Homo sapiens GN=HIST1H4A PE=1 SV=2 - [H4_HUMAN]	ENSP00000476824	P62805	1.784160043	1.960381758	2.172168563	2.323679014	HIST1H4F
Histone H4 OS=Homo sapiens GN=HIST1H4A PE=1 SV=2 - [H4_HUMAN]	ENSP00000476824	P62805	1.784160043	1.960381758	2.172168563	2.323679014	HIST1H4H
Histone H4 OS=Homo sapiens GN=HIST1H4A PE=1 SV=2 - [H4_HUMAN]	ENSP00000476824	P62805	1.784160043	1.960381758	2.172168563	2.323679014	HIST1H4I
Histone H4 OS=Homo sapiens GN=HIST1H4A PE=1 SV=2 - [H4_HUMAN]	ENSP00000476824	P62805	1.784160043	1.960381758	2.172168563	2.323679014	HIST1H4J
Histone H4 OS=Homo sapiens GN=HIST1H4A PE=1 SV=2 - [H4_HUMAN]	ENSP00000476824	P62805	1.784160043	1.960381758	2.172168563	2.323679014	HIST1H4K
Histone H4 OS=Homo sapiens GN=HIST1H4A PE=1 SV=2 - [H4_HUMAN]	ENSP00000476824	P62805	1.784160043	1.960381758	2.172168563	2.323679014	HIST1H4L
Histone H3.2 OS=Homo sapiens GN=HIST2H3A PE=1 SV=3 - [H32_HUMAN]	ENSP00000463995	Q71DI3	1.771240736	1.740352367	2.072844065	1.931687716	HIST2H3A
Histone H3.2 OS=Homo sapiens GN=HIST2H3A PE=1 SV=3 - [H32_HUMAN]	ENSP00000463995	Q71DI3	1.771240736	1.740352367	2.072844065	1.931687716	HIST2H3C
Histone H3.2 OS=Homo sapiens GN=HIST2H3A PE=1 SV=3 - [H32_HUMAN]	ENSP00000463995	Q71DI3	1.771240736	1.740352367	2.072844065	1.931687716	HIST2H3D
Histone H4 OS=Homo sapiens GN=HIST1H4A PE=1 SV=2 - [H4_HUMAN]	ENSP00000476824	P62805	1.784160043	1.960381758	2.172168563	2.323679014	HIST2H4A
Histone H4 OS=Homo sapiens GN=HIST1H4A PE=1 SV=2 - [H4_HUMAN]	ENSP00000476824	P62805	1.784160043	1.960381758	2.172168563	2.323679014	HIST2H4B
Histone H4 OS=Homo sapiens GN=HIST1H4A PE=1 SV=2 - [H4_HUMAN]	ENSP00000476824	P62805	1.784160043	1.960381758	2.172168563	2.323679014	HIST4H4
Integrin alpha-M OS=Homo sapiens GN=ITGAM PE=1 SV=2 - [ITAM_HUMAN]	ENSP00000441691	P11215	1.093825333	0.948178503	0.829550669	0.958952616	ITGAM
Inositol 1,4,5-trisphosphate receptor type 2 OS=Homo sapiens GN=ITPR2 PE=1 SV=2 - [ITPR2_HUMAN]	ENSP00000370744	Q14571	1.204289124	1.128797951	1.107464662	1.220349872	ITPR2

Note: Upregulated proteins (above 1.2-fold expression of the naïve control) are shown in red and downregulated proteins (below 0.83-fold expression of the naïve control) are shown in green.

Table 1 (continued)

KH domain-containing, RNA-binding, signal transduction-associated protein 3 (Fragment) OS=Homo sapiens GN=KHDRBS3 PE=1 SV=2 - [E5RG12_HUMAN]	ENSP00000430284	E5RG12	1.204517292	1.194785319	1.167175046	1.135787017	KHDRBS3
Keratin, type I cytoskeletal 17 (Fragment) OS=Homo sapiens GN=KRT17 PE=1 SV=1 - [K7EPJ9_HUMAN]	ENSP00000467418	K7EPJ9	1.062276013	1.022441312	1.247848252	1.171862206	KRT17
Uncharacterized protein C12orf55 OS=Homo sapiens GN=C12orf55 PE=4 SV=4 - [E9PJL5_HUMAN]	ENSP00000431759	E9PJL5	1.513583318	0.929137772	1.20967811	1.195255884	LOC101928871
Microtubule-associated protein 1A OS=Homo sapiens GN=MAP1A PE=1 SV=6 - [MAP1A_HUMAN]	ENSP00000300231	P78559	0.875826478	0.805108528	0.794477484	0.793799135	MAP1A
Myb-binding protein 1A OS=Homo sapiens GN=MYBBP1A PE=1 SV=2 - [MBB1A_HUMAN]	ENSP00000370968	Q9BQG0	1.076499444	1.206942358	1.111468727	1.077427925	MYBBP1A
Condensin-2 complex subunit D3 OS=Homo sapiens GN=NCAPD3 PE=1 SV=2 - [CNDD3_HUMAN]	ENSP00000433681	P42695	0.783925027	0.796345366	0.860997555	0.881569865	NCAPD3
NHP2-like protein 1 OS=Homo sapiens GN=NHP2L1 PE=1 SV=3 - [NH2L1_HUMAN]	ENSP00000383949	P55769	1.453540038	1.349218797	1.373663698	1.326709606	NHP2L1
Nucleolar complex protein 3 homolog OS=Homo sapiens GN=NOC3L PE=1 SV=1 - [A6NJZ9_HUMAN]	ENSP00000360401	A6NJZ9	1.225057984	1.1956667	1.046542081	1.109198717	NOC3L
Non-POU domain-containing octamer-binding protein (Fragment) OS=Homo sapiens GN=NONO PE=1 SV=1 - [C9IZL7_HUMAN]	ENSP00000406673	C9IZL7	0.920710188	0.880105568	0.75136696	0.999206525	NONO
Nucleophosmin OS=Homo sapiens GN=NPM1 PE=1 SV=2 - [NPM_HUMAN]	ENSP00000428755	P06748	0.804719697	0.854502403	0.868195381	0.890603396	NPM1
2-oxoglutarate dehydrogenase, mitochondrial OS=Homo sapiens GN=OGDH PE=1 SV=3 - [ODO1_HUMAN]	ENSP00000392878	Q02218	1.094326775	1.148259559	1.228246707	1.210921101	OGDH
Protein RRP5 homolog OS=Homo sapiens GN=PDCD11 PE=1 SV=3 - [RRP5_HUMAN]	ENSP00000358812	Q14690	0.708811172	0.701105862	0.856758752	0.846150807	PDCD11
Isoform 4 of Piezo-type mechanosensitive ion channel component 2 OS=Homo sapiens GN=PIEZO2 - [PIEZ2_HUMAN]	ENSP00000463094	Q9H5I5-4	1.274110488	1.175494098	1.177873784	1.040357004	PIEZO2
Phosphoinositide phospholipase C (Fragment) OS=Homo sapiens GN=PLCB1 PE=4 SV=1 - [H0YCJ2_HUMAN]	ENSP00000431704	H0YCJ2	1.155486143	1.089485058	1.262176882	1.329957498	PLCB1
Inactive phospholipase C-like protein 2 OS=Homo sapiens GN=PLCL2 PE=1 SV=2 - [PLCL2_HUMAN]	ENSP00000412836	Q9UPR0	2.61807713	2.278039918	2.457023769	2.956838363	PLCL2
Ribosomal protein L19 OS=Homo sapiens GN=RPL19 PE=1 SV=1 - [J3QR09_HUMAN]	ENSP00000463985	J3QR09	1.238365956	1.224952072	1.163249705	1.137235374	RPL19
40S ribosomal protein S15 OS=Homo sapiens GN=RPS15 PE=1 SV=2 - [K7EM56_HUMAN]	ENSP00000474970	K7EM56	1.204518602	1.16517906	1.315604067	1.125009282	RPS15
Isoform 2 of Ribosomal protein S6 kinase-like 1 OS=Homo sapiens GN=RPS6KL1 - [RPKL1_HUMAN]	ENSP00000450660	Q9Y6S9-2	1.431013489	1.459189196	0.989579973	1.157354049	RPS6KL1
Isoform 2 of Ryanodine receptor 1 OS=Homo sapiens GN=RYR1 - [RYR1_HUMAN]	ENSP00000347667	P21817-2	1.031954665	0.981386838	0.999560378	0.828242976	RYR1
Protein S100-A6 (Fragment) OS=Homo sapiens GN=S100A6 PE=1 SV=1 - [R4GN98_HUMAN]	ENSP00000473547	R4GN98	1.088185196	0.938134058	0.994601666	0.634291315	S100A6
ADP/ATP translocase 1 OS=Homo sapiens GN=SLC25A4 PE=1 SV=1 - [V9GYG0_HUMAN]	ENSP00000476711	V9GYG0	1.003891449	0.937431762	0.898068342	0.829477749	SLC25A4
WD40 repeat-containing protein SMU1 OS=Homo sapiens GN=SMU1 PE=1 SV=2 - [SMU1_HUMAN]	ENSP00000380336	Q2TAY7	1.126229739	1.095912818	1.022596249	1.512638485	SMU1
Serine palmitoyltransferase 3 OS=Homo sapiens GN=SPTLC3 PE=1 SV=3 - [SPTC3_HUMAN]	ENSP00000381968	Q9NUV7	1.413312594	1.314942475	1.675235307	1.40581247	SPTLC3
Squalene monooxygenase OS=Homo sapiens GN=SQLE PE=1 SV=3 - [ERG1_HUMAN]	ENSP00000265896	Q14534	1.122685581	1.243574947	1.087534102	1.117460656	SQLE
Transmembrane protein 63B (Fragment) OS=Homo sapiens GN=TMEM63B PE=1 SV=1 - [H3BLW6_HUMAN]	ENSP00000360960	H3BLW6	1.454865059	1.417457784	1.587039619	1.724742711	TMEM63B
Isoform 12 of Titin OS=Homo sapiens GN=TTN - [TITIN_HUMAN]	ENSP00000467141	Q8WZ42-12	0.8798485	0.823006585	0.935878876	0.943042145	TTN
Protein Wiz OS=Homo sapiens GN=WIZ PE=1 SV=2 - [WIZ_HUMAN]	ENSP00000445824	O95785	1.128844277	1.095648443	1.208689644	1.197310506	WIZ
Zinc finger MYM-type protein 6 OS=Homo sapiens GN=ZMYM6 PE=2 SV=2 - [ZMYM6_HUMAN]	ENSP00000362437	O95789	0.795319219	0.689734822	0.798711907	0.913133542	ZMYM6
Zinc finger protein 570 OS=Homo sapiens GN=ZNF570 PE=4 SV=1 - [K7EP39_HUMAN]	ENSP00000467218	K7EP39	0.70175368	0.850511342	0.847634046	0.697821255	ZNF570

Note: Upregulated proteins (above 1.2-fold expression of the naïve control) are shown in red and downregulated proteins (below 0.83-fold expression of the naïve control) are shown in green.

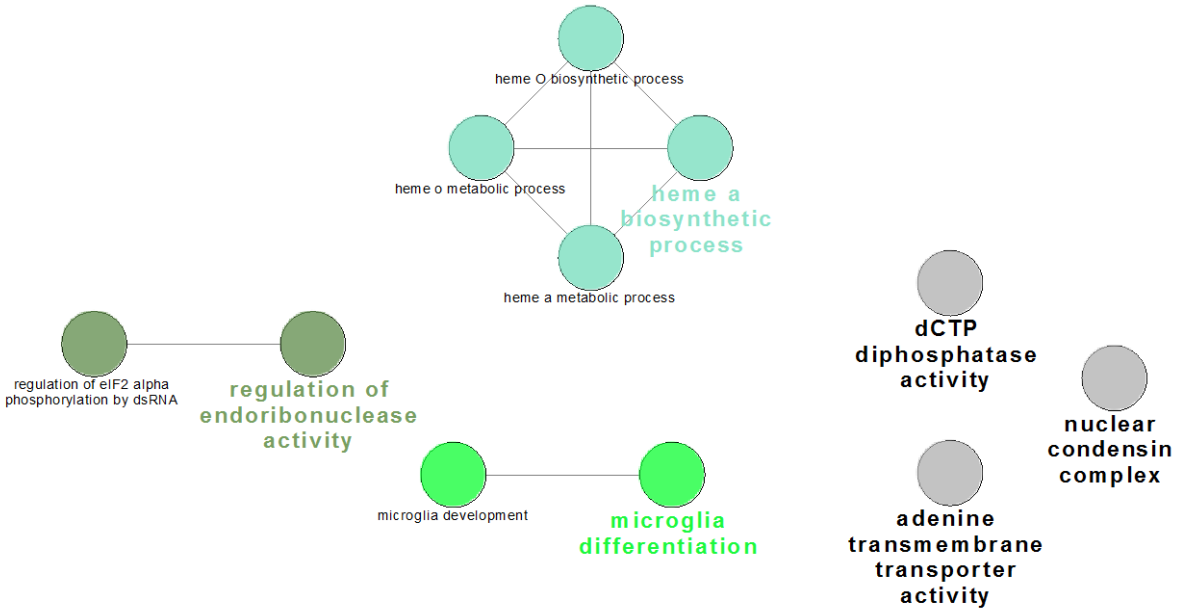

Figure 6. GO Term Pathway Analysis of Downregulated Proteins following JP-8 Exposure

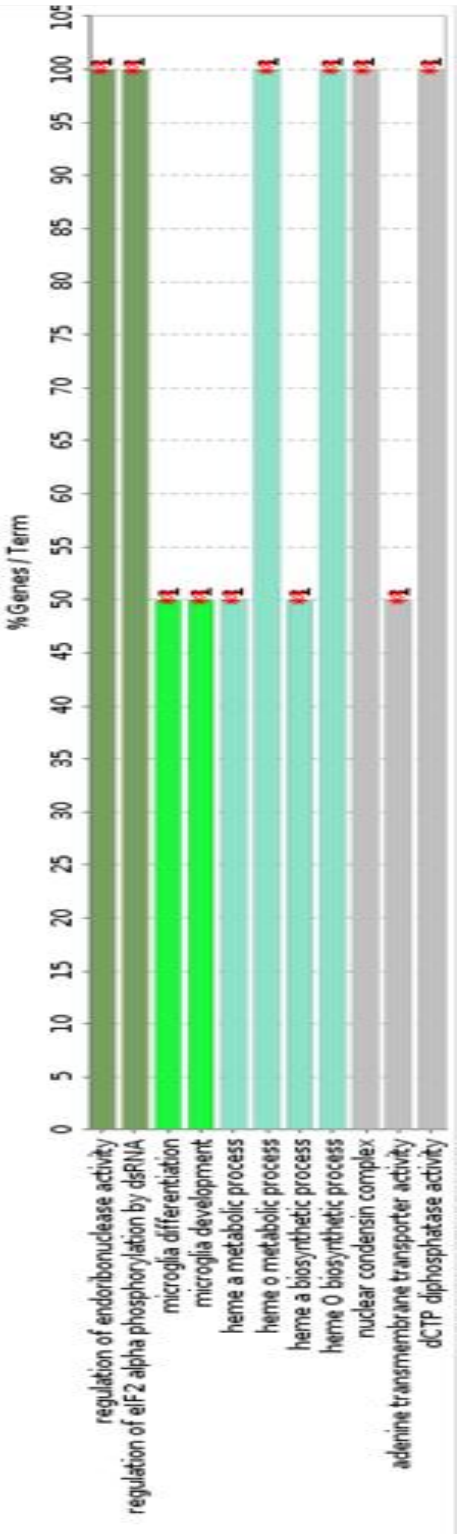

Figure 7. GO Term Bar Chart Analysis of Downregulated Proteins following JP-8 Exposure

4.2.5 Conclusion: In conclusion, JP-8 had marginal cytotoxic effects on HEI-OC1 cells at the highest dose of 500 ppm, namely upregulation of histones involved in chromatin remodeling as a result of oxidative stress. Although effects were not dramatic, a dose response was apparent. It remains to be determined if the dose of JP-8 needs to be increased to account for potential leakage of JP-8 into the cell culture vessel. Additionally, it would be interesting to determine if JP-8 accelerates cytotoxicity by co-exposure to oligomycin, a simulant of hearing loss-associated oxidative stress.

4.3 *In Vitro* Cytotoxic Response of Cochlear Cells to JP-8 Exposure

The present study investigated the effects of JP-8 and five key hydrocarbons of the JP-8 mixture which are known to affect hearing: decane, nonane, toluene, ethylbenzene, and m-xylene, in the presence and absence of oligomycin, on apoptosis and necrosis. Oligomycin inhibits ATP synthase by blocking its proton channel, which is necessary for oxidative phosphorylation of adenosine diphosphate to adenosine triphosphate (ADP to ATP, energy production process). Hence, oligomycin is often used as a surrogate for noise-induced energy depletion, *in vitro* (Chen *et al.*, 2012; Kalinec *et al.*, 2003).

4.3.1 Cell Culture and Exposure Methods. HEI-OC1 cells were seeded at a density of 15,000 cells per well, on three Falcon™ black-walled, clear bottom 96 well tissue culture plates (BD Biosciences, San Jose CA) in 200 µl high glucose DMEM with 10 percent fetal bovine serum (FBS). The cells were allowed to proliferate in an incubator with 5 percent CO_2 at 33°C, to approximately 80 percent confluency before the experimental exposures.

When cells reached 70 to 80 percent confluency, media was carefully removed and replaced with serum free media, containing either JP-8 (50 or 1000 ppm); decane, nonane, toluene, ethylbenzene, m-xylene (5 or 500 ppm); or gentamicin (1 or 100 µM); all with or without 1 µM oligomycin. Oligomycin dilutions were made from a 5mM oligomycin stock in dimethyl sulfoxide (DMSO). In addition, two sets of cells were exposed to oligomycin at 1 or 100 µM, to assess the compound effect. In control wells, as well as those wells containing JP-8 or key hydrocarbons without the presence of oligomycin, DMSO was added to match the amount used in the oligomycin-exposed wells.

To examine the effect of FBS content on the dose response of JP-8, HEI-OC1 cells were seeded at 15,000 cells per well as described above. When the cells reached 80 percent confluency (overnight), regular media (see above) was removed and replaced with media containing either 0, 1, or 10 percent FBS; concentrations of JP-8 ranging from 50 to 3000 ppm; and 0.5 percent DMSO for 24 hours.

4.3.2 Cell Viability Assays. To assess cell health after exposures, the Promega ApoTox-Glo™ Triplex Assay (Madison WI) was used. This multi-parametric assay measures viability, cytotoxicity, and caspase activation within a single assay well. Viability and cytotoxicity are measured by a fluorogenic, cell-permeable peptide substrate that enters intact cells, where it is

cleaved by live-cell proteases, generating a fluorescent signal. These live-cell proteases become inactive upon loss of membrane integrity and leakage into surrounding medium. A second fluorogenic cell-impermeable peptide substrate is then used to measure dead-cell protease. Third, a luminogenic caspase-3/7 substrate, which undergoes caspase cleavage, generates a luminescent signal upon activation of the caspase cascade. The signals emitted are proportional to the number of live cells, dead cells, and level of caspase activity (apoptosis), respectively. At 2, 4, and 24 hours after exposure, these activities were assayed following the manufacturer's instructions. Fluorescence and luminescence values were acquired using a FlexStation 3 multi-mode plate reader (Molecular Devices, Sunnyvale CA). The results were normalized to background measurements.

Viability was also assessed using the CellTiter 96® AQueous Non-Radioactive Cell Proliferation Assay (Promega Corporation, Madison WI), consisting of a solution of a tetrazolium compound [3-(4,5-dimethylthiazol-2-yl)-5-(3-carboxymethoxyphenyl)-2-(4-sulfophenyl)-2H-tetrazolium, inner salt; MTS] and an electron coupling reagent. MTS is bioreduced by cells into a formazan product. The absorbance of the formazan product at 490 nm is measured directly without additional processing. The conversion of MTS into formazan is accomplished by dehydrogenase enzymes found in metabolically active cells. Therefore, quantity of formazan product is directly proportional to the number of living cells in culture.

For each assay, statistical significance of differences ($p \leq 0.05$) were evaluated using one-way analysis of variance (ANOVA) tests performed using Microsoft® Excel (Redmond WA).

4.3.3 Results. Results are shown in Figures 8 through 11. After 2 hours of exposure, all compounds exhibited more live to dead cells, even in the presence of oligomycin, relative to untreated controls (i.e., less than one in Figures 8 and 9). Non-lethal cytotoxic effects may be occurring at 2 hours, but actual changes in membrane integrity may have not yet begun at this time point. At 4 and 24 hours, a general increase in cell death was seen across compounds; however, in most cases, there was little difference from background. Apoptosis contributes to cell death in the high dose exposures across compounds, as well as the low dose exposure for ethylbenzene (Figure 10). However, based on Figures 9 and 11, necrosis contributed more to cell death from exposure to the positive control, gentamicin, than apoptosis. Of the compounds tested, m-xylene, ethylbenzene, and toluene exhibited the greatest toxicity. In general, oligomycin enhanced cytotoxicity when combined with hydrocarbons. Although there is a clear dose-response from oligomycin alone, when it is combined with gentamicin, it reduces caspase activity (Figure 11).

The effect of FBS content on JP-8 dose-response is shown in Figure 12. At each JP-8 concentration, with the exception of 3000 ppm, significant differences in mean viability occur between cells incubated with different FBS concentrations, based on analysis with a one-factor ANOVA (significance between groups not shown in figure). Cell viability more consistently decreased with increased JP-8 concentration when cells were incubated with 1 percent FBS.

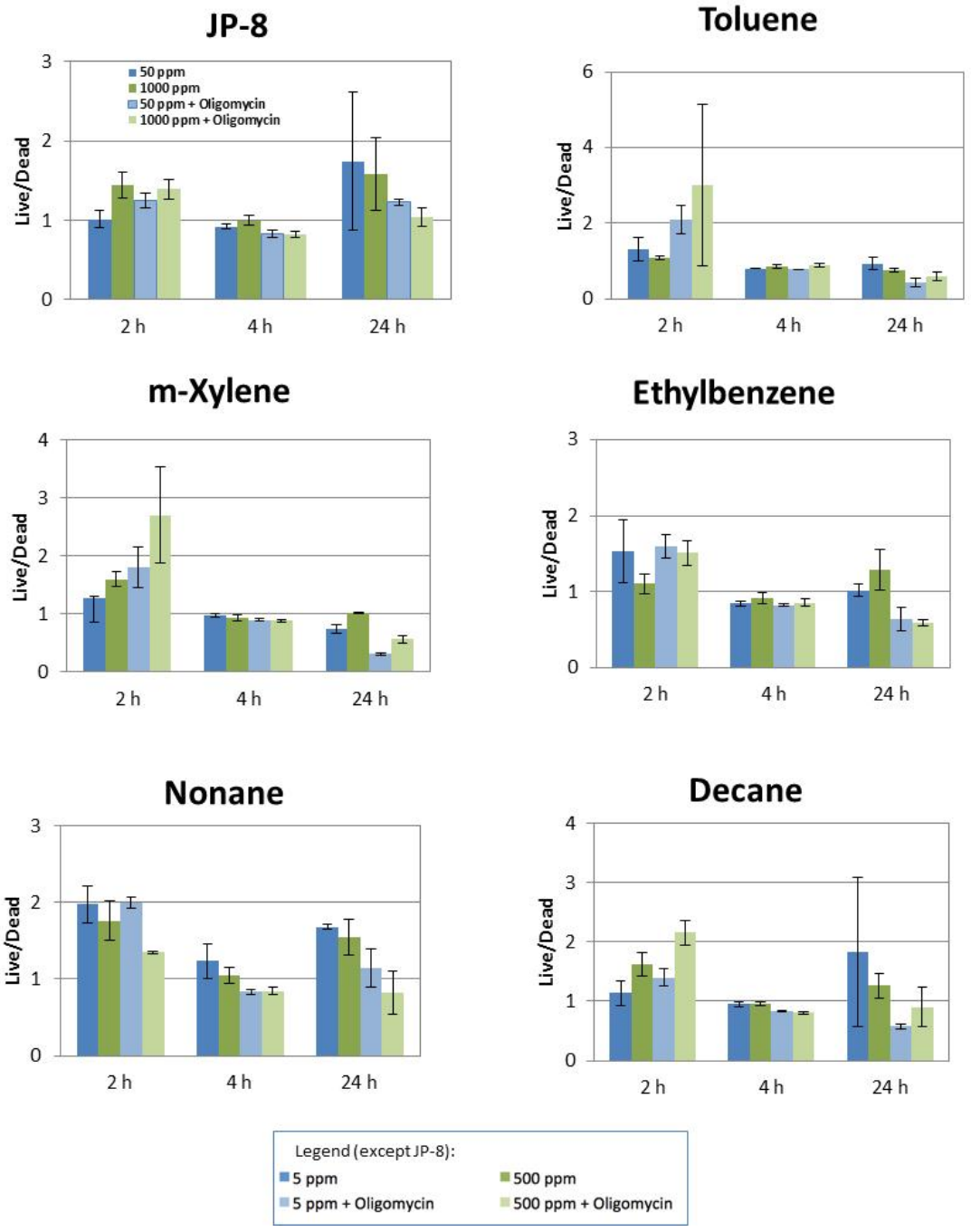

Figure 8. Fold Change over Background of Viability/Cytotoxicity: JP-8 and Key Hydrocarbons. Variability in background viability and cytotoxicity measurements were less than 1 percent and 10 percent, respectively (n=4). Note: JP-8 has a different legend than the individual hydrocarbons. Oligomycin was dosed at 1 µM as a noise surrogate.

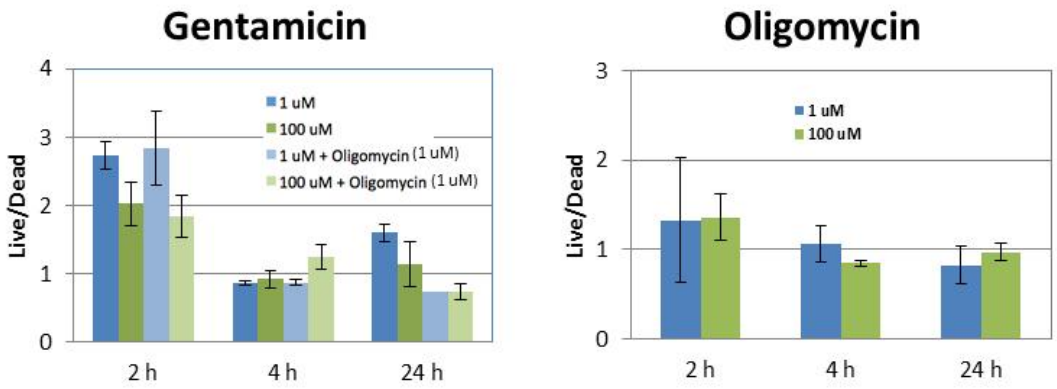

Figure 9. Fold Change over Background of Viability/Cytotoxicity: Gentamicin and Oligomycin. Variability in background viability and cytotoxicity measurements were less than 1 percent and 10 percent, respectively (n=4). Oligomycin served as a noise surrogate.

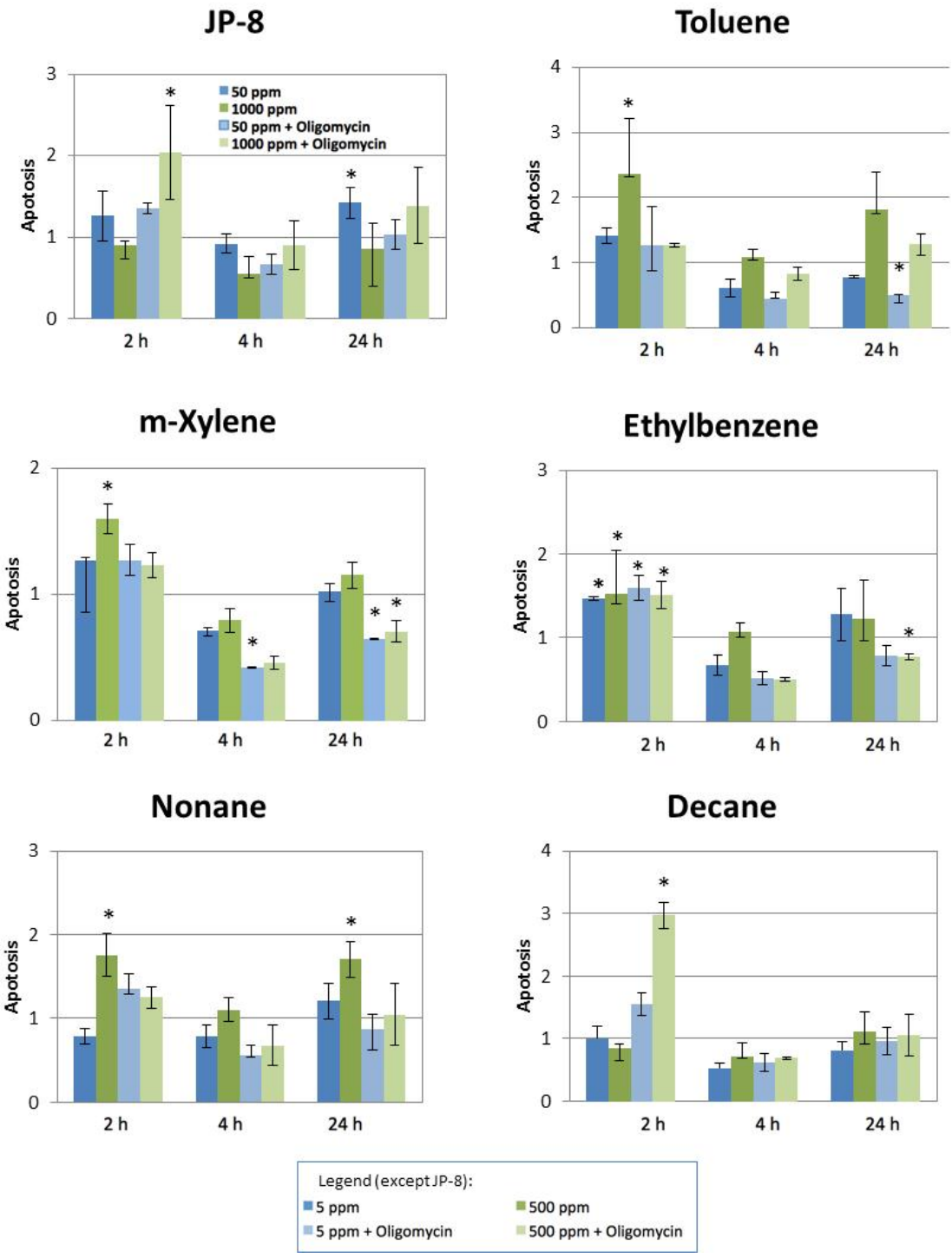

Figure 10. Fold Change over Background of Caspase Activity: JP-8 and Key Hydrocarbons. Results are shown for JP-8 or hydrocarbon, alone and in the presence of 0.1 µM oligomycin, which served as a noise surrogate. Note: *$p \leq 0.05$, n=4

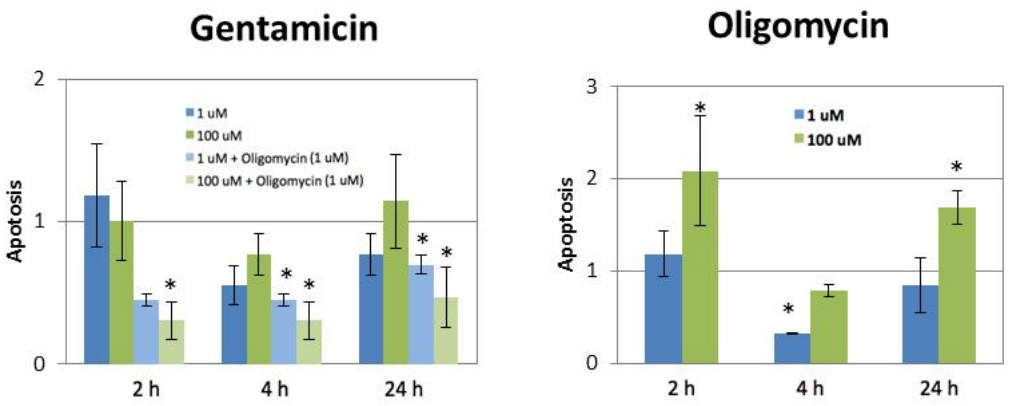

Figure 11. Fold Change over Background of Caspase Activity: Gentamicin and Oligomycin. Oligomycin served as a noise surrogate. Note: *p ≤ 0.05, n=4

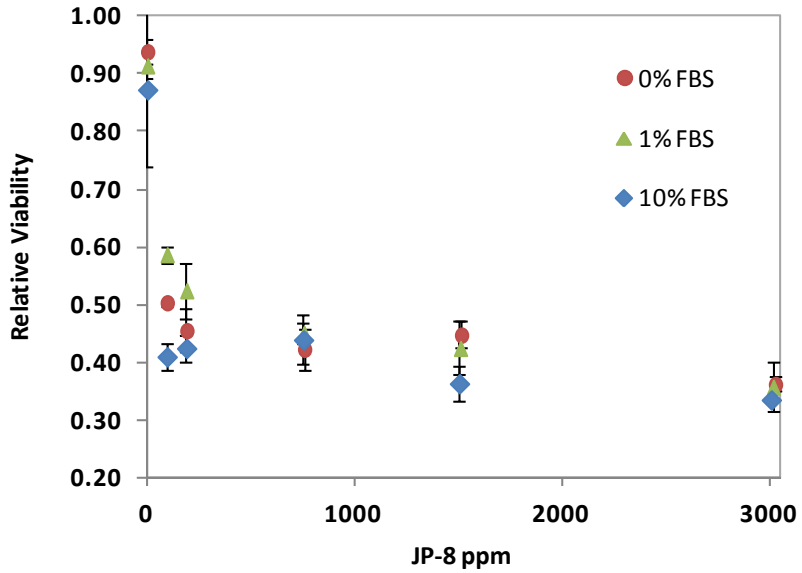

Figure 12. Effect of FBS Content on JP-8 Dose-Response in HEI-OC1 cells. Relative changes in viability based on MTS assay (n=4) in HEI-OC1 cells exposed for 4 hours in media containing 0, 93, 186, 750, 1500, or 3000 ppm JP-8 in 0.5 percent DMSO; and either 0, 1, or 10 percent FBS. Significant differences among means were found in the 0, 93, 186, 750, and 1500 ppm JP-8 groups.

4.3.4 Conclusion. Overall, the results from this study are in agreement with those from the proteomic assessment. Little toxicity in HEI-OC1 cells was seen from JP-8. The increase in live/dead ratios at the earliest observation suggests that two hours may not be a suitable time

point for these assays. Early induction of protective cellular mechanisms may explain the lack of cytotoxic effects at the two-hour time point. This is consistent with the upregulation of numerous histones, discussed above in Section 4.2.2.

By using the ApoTox® assay, we demonstrated that apoptosis and necrosis induced by these compounds was enhanced by the presence of oligomycin. However, alone the components showed little impact. Collectively, these findings support the proteomic results in Section 4.2.2, demonstrating JP-8, at levels relevant to exposures of AF personnel, had minimal effects on cochlear hair cells.

In an effort to screen the toxicity of multiple compounds, only two concentrations of each were used. In future assays, serial dilutions of fewer compounds is advised. Using only two concentrations can be problematic due to factors including biological variation in response and physiochemical concerns, such as solubility. Here, the exposure chemicals were delivered via sound waves, using the ECHO^{TM} liquid handler. Given the high volatility of the hydrocarbons used, it is possible that the delivered aliquots are not well mixed into the media of the designation plate before being sealed and placed into the incubator, where further chemical loss to the well headspace may have occurred.

Serum binding to hydrocarbons may also affect dose delivery. Differences were observed in the JP-8 dose-responses when combined with 0, 1, or 10 percent FBS (Figure 12). The clearest dose-response was seen with 1 percent FBS. Therefore, on-going studies are using 1 percent FBS in the exposure media.

Interestingly, oligomycin, which acts via energy depletion, demonstrated greater toxicity at 3 hours than at 24 hours. The media used contained high glucose levels. Glucose, to some extent, may have reduced ATP depletion by providing an additional energy source.

5.0 FUTURE WORK

For humans, central auditory processing dysfunction, as opposed to cochlear hair cell damage, may be among the first signs of hearing loss (Bamiou *et al.*, 2000). In the absence of peripheral (cochlear) impairment, a significant CAPD was detected among the jet fuel and jet fuel plus noise groups of Long-Evans rats (Guthrie *et al.*, 2014). This indicates that CAPD may be part of the ototoxic profile of jet fuel exposure. This line of thinking is supported by a recent study indicating that military personnel at risk for exposure to jet fuel combined with attenuated noise exhibited normal hearing but suffered with a CAPD. Royal Air Force pilots were poor at auditory frequency discrimination tasks, which were associated with a CAPD that manifested as an impaired ability to recognize speech in background listening situations (Hope *et al.*, 2013). In addition, altered growth functions of the brainstem components of the ABR are characteristic of aging (Boettcher *et al.*, 1993; Popelar *et al.*, 2006; Zhou *et al.*, 2006).

These data are consistent with our current *in vitro* findings, showing little if any effect of JP-8 or JP-8 components on toxicity endpoints such as cell viability or proteomic markers. We thus will be considering potential interactions between jet fuel and noise that may occur at a higher signal

processing level via in vivo strudies, mentioned below, rather than just at the level of cell toxicity.

5.1 Potential Model Improvements

The current model uses arbitrary values for parameters such as rate constants. These parameters ultimately need to be determined by calibrating and validating the model against relevant *in vitro* (and *in vivo*) data, both from the present project and available from the literature.

Currently, the model presents a description of the impact of noise and a single chemical on oxidative stress-mediated hair cell inactivation and loss. In order to describe the effect of multiple chemical components or mixtures, such as jet fuel, equation (5) can be replaced with equation (1), and rate constants k_i for free radical production by each chemical can be introduced. Chemical concentrations C_i at the cochlea for each jet fuel component that may generate free radicals can be predicted by a jet fuel PBPK model currently under development.

The model is created with a necessary simplification of a complex situation. For example, there are multiple anti-oxidants, with specific affinities for specific free and lipid radicals, which have all been "lumped" together in the present model as GSH. The assumption is that these pathways chosen (GSH, etc.) dominate the events associated with jet fuel chemical exposure. Similarly, multiple radical types have also been treated as a single entity. As more *in vitro* and *in vivo* data become available, specific interactions of more dominant radical metabolites can be separated from this generic interaction and individually parameterized.

The effects of oxidative stress on cochlear hair cells need to be interfaced with other aspects of hearing loss, such as damage to the brainstem auditory pathway. By blocking voltage-dependent calcium channels (VDCC), fuel exposure may reduce the middle ear reflex (MER), which normally protects the auditory pathway from the effects of excessive noise by physically reducing the sound that reaches the cochlea (Maguin *et al.*, 2009). In addition, noise induces the CAP to self-regulate, and this ability may be compromised by the reduced synaptic excitability associated with fuel exposure (Pilati *et al.*, 2012).

Brain stem effects (CAPD) have been implicated in rats exposed to jet fuel or jet fuel plus noise exposure without apparent reductions in hearing acuity (Guthrie *et al.*, 2014). Also, toluene, a fuel component, has been shown to depress the auditory nervous system in Long-Evans rats, interfering with muscle contractions which help to dampen noise (MER), (see Figure 13), which could explain increases in NIHL with concurrent toluene exposure (Maguin *et al.*, 2009; Venet *et al.*, 2011).

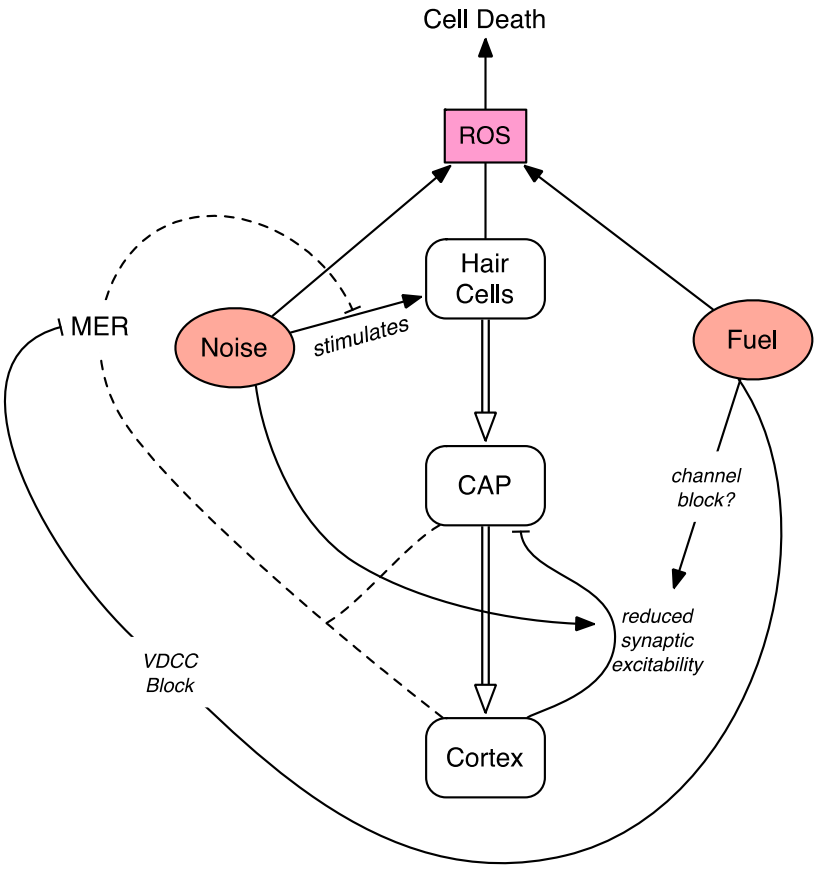

Figure 13. Schematic of the Effect of Fuel Exposure on a Number of Pathways, and Regulatory Mechanisms associated with the Response of the Auditory Pathway to Noise. CAP: central auditory processing; MER: middle ear reflex; ROS: reactive oxygen species; VDCC: voltage-dependent calcium channels

5.2 *In Vitro /In Vivo* Studies

In order to explore interactions between jet fuel and noise, it is necessary to understand underlying mechanisms, assess the potential for further deterioration, and explore means to ameliorate the condition. Effects on the central auditory pathway, as well as on hair cells, should be explored thoroughly.

In addition the HEI-OC1 cells, the neuroblast cell line, VOT-N33, and the otic epithelial cell line, VOT-E36, have been kindly provided by Dr. Matthew C. Holley (Department of Biomedical Science, University of Sheffield, England). These cell lines were originally derived from similar regions of the ventral otocyst of the immortomouse at embryonic day 10.5 (Lawoko-Kerali *et al.*, 2004). As experimental models, the VOT-E36 and VOT-N33 cell lines express a number of sensory epithelia and spiral ganglion specific markers making them useful tools for the *in vitro* study of the influence and the mechanism of ototoxic agent on auditory cells. An initial dose response study with HEI-OC1, VOT-E36, and VOT-N33 cells in 384 well

plates was attempted. Results were not reliable due to a much slower growth rate of VOT-E36 and a loss of too many of cells during washes; however the initial results suggest greater sensitivity of the VOT cell lines to JP-8 and constituents than seen in HEI-OC1. Therefore, dose response JP-8 cytotoxicity studies in these lines in separate 96 well plates are currently underway.

Effects on the central auditory pathway, as well as on hair cells, should be explored thoroughly, especially given the limited cytotoxicity seen *in vitro*. Guthrie *et al.* (2014) studied the effects of JP-8 and noise *in vivo* and found that the effects of JP-8 alone attributed mainly to deregulation of the central auditory nervous system (CANS). They stated, "…it is tempting to speculate that jet fuel or jet fuel + noise exposure induced a partially accelerated aging phenotype of the CANS." Aging of the CANS is related to alterations in gamma-aminobutyric acid A receptor ($GABA_AR$) changes (Caspary *et al.*, 2008). The slope of the stimulus-response growth function of the CANS has been correlated with the level of 5- hydroxyindoleacetic acid, a serotonin metabolite, in cerebrospinal fluid (Hegerl and Juckel, 1993). In addition, gene expression analysis of JP-8 exposed rats compared to the control group revealed a modulation of several genes, including GABA transporter 3 (GAT-3) (Lin *et al.*, 2001). Therefore we propose collecting tissue samples from upcoming JP-8 studies in rats and performing immunohistochemistry to quantify changes in the inhibitory signaling system, namely $GABA_AR$ subtypes, GABA transaminase, and serotonin receptors in the brainstem nuclei.

5.3 PBPK Parameterization

For a tissue compartment to be successfully described in a PBPK model, the following should be measured or calculated: volume of the tissue (fraction of body weight), the blood flow to the tissue (fraction of cardiac output), and partitioning of the chemical into the tissue (partition coefficient, PC, unitless). Cochlea blood flow is well characterized in the literature (Hillerdal, 1987; Hillerdal *et al.*, 1987; Larsen *et al.*, 1984). The remaining parameters are not available from literature sources and were only estimated in a preliminary model (Robinson *et al.*, 2013).

Since central auditory pathway dysfunction has been found as an early indicator of JP-8 hearing loss in rats (Guthrie *et al.*, 2014), the PBPK model must be expanded to contain not only a cochlea compartment, but also expand to a brainstem, temporal lobe (central auditory pathway regions), and frontal lobe (representing the remainder of the brain) compartments. Incorporation of hearing pathway tissues into the model requires the following parameters for each tissue: weight (fraction of body weight), partition coefficients, and tissue composition (water, protein, neutral lipid, neutral phospholipid, and acidic phospholipid contents). Methods are being developed to measure each of these parameters.

6.0 REFERENCES

Agrawal, Y., Platz, E.A. and Niparko, J.K. 2008. Prevalence of hearing loss and differences by demographic characteristics among US adults: data from the National Health and Nutrition Examination Survey, 1999-2004. Arch Intern Med 168(14): 1522-1530.

Ambrosini, A., Rossi, P., De Pasqua, V., Pierelli, F. and Schoenen, J. 2003. Lack of habituation causes high intensity dependence of auditory evoked cortical potentials in migraine. Brain 126(Pt 9): 2009-2015.

Bamiou, D.E., Liasis, A., Boyd, S., Cohen, M. and Raglan, E. 2000. Central auditory processing disorder as the presenting manifestation of subtle brain pathology. Audiology 39(3): 168-172.

Boettcher, F.A., Mills, J.H. and Norton, B.L. 1993. Age-related changes in auditory evoked potentials of gerbils. I. Response amplitudes. Hear Res 71(1-2): 137-145.

Boulares, A.H., Contreras, F.J., Espinoza, L.A. and Smulson, M.E. 2002. Roles of oxidative stress and glutathione depletion in JP-8 jet fuel- induced apoptosis in rat lung epithelial cells. Toxicol Appl Pharmacol 180(2): 92-99.

Byczkowski, J.Z., Flemming, C.D., Curran, M.A., Miller, C.R., Schmidt, W.J., Moghaddam, A.P. and Channel, S.R. 1997. Physiologically based pharmacodynamic modeling of chemically induced oxidative stress. Wright-Patterson AFB, OH: Armstrong Laboratory, Toxicology Division. AL/OE-TR-1997-0130, ADA362299.

Campo, P., Lataye, R., Loquet, G. and Bonnet, P. 2001. Styrene-induced hearing loss: a membrane insult. Hear Res 154(1-2): 170-180.

Caspary, D.M., Ling, L., Turner, J.G. and Hughes, L.F. 2008. Inhibitory neurotransmission, plasticity and aging in the mammalian central auditory system. J Exp Biol 211(Pt 11): 1781-1791.

Chen, F.Q., Zheng, H.W., Hill, K. and Sha, S.H. 2012. Traumatic noise activates Rho-family GTPases through transient cellular energy depletion. J Neurosci 32(36): 12421-12430.

Fechter, L.D. 1999. Mechanisms of ototoxicity by chemical contaminants: Prospects for intervention. Noise Health 1(2): 10-27.

Fechter, L.D. 2005. Oxidative stress: a potential basis for potentiation of noise-induced hearing loss. Environ Toxicol Pharmacol 19(3): 543-546.

Fechter, L.D., Fisher, J.W., Chapman, G.D., Mokashi, V.P., Ortiz, P.A., Reboulet, J.E., Stubbs, J.E., Lear, A.M., McInturf, S.M., Prues, S.L., Gearhart, C.A., Fulton, S. and Mattie, D.R. 2012. Subchronic JP-8 jet fuel exposure enhances vulnerability to noise-induced hearing loss in rats. J Toxicol Environ Health A 75(5): 299-317.

Fechter, L.D., Gearhart, C., Fulton, S., Campbell, J., Fisher, J., Na, K., Cocker, D., Nelson-Miller, A., Moon, P. and Pouyatos, B. 2007. JP-8 jet fuel can promote auditory impairment resulting from subsequent noise exposure in rats. Toxicol Sci 98(2): 510-525.

Fechter, L.D., Gearhart, C.A. and Fulton, S. 2010. Ototoxic potential of JP-8 and a Fischer-Tropsch synthetic jet fuel following subacute inhalation exposure in rats. Toxicol Sci 116(1): 239-248.

Gallinat, J., Bottlender, R., Juckel, G., Munke-Puchner, A., Stotz, G., Kuss, H.J., Mavrogiorgou, P. and Hegerl, U. 2000. The loudness dependency of the auditory evoked N1/P2-component as a predictor of the acute SSRI response in depression. Psychopharmacology (Berl) 148(4): 404-411.

Guest, M., Boggess, M., Attia, J., D'Este, C., Brown, A., Gibson, R., Tavener, M., Gardner, I., Harrex, W., Horsley, K. and Ross, J. 2010. Hearing impairment in F-111 maintenance workers: the study of health outcomes in aircraft maintenance personnel (SHOAMP) general health and medical study. Am J Ind Med 53(11): 1159-1169.

Guthrie, O.W., Xu, H., Wong, B.A., McInturf, S.M., Reboulet, J.E., Ortiz, P.A. and Mattie, D.R. 2014. Exposure to low levels of jet-propulsion fuel impairs brainstem encoding of stimulus intensity. J Toxicol Environ Health A 77(5): 261-280.

Hegerl, U. and Juckel, G. 1993. Intensity dependence of auditory evoked potentials as an indicator of central serotonergic neurotransmission: a new hypothesis. Biol Psychiatry 33(3): 173-187.

Henderson, D., Bielefeld, E.C., Harris, K.C. and Hu, B.H. 2006. The role of oxidative stress in noise-induced hearing loss. Ear Hear 27(1): 1-19.

Hillerdal, M. 1987. Cochlear blood flow in the rat. A methodological evaluation of the microsphere method. Hear Res 27(1): 27-35.

Hillerdal, M., Sperber, G.O. and Bill, A. 1987. The microsphere method for measuring low blood flows: theory and computer simulations applied to findings in the rat cochlea. Acta Physiol Scand 130(2): 229-235.

Hope, A.J., Luxon, L.M. and Bamiou, D.E. 2013. Effects of chronic noise exposure on speech-in-noise perception in the presence of normal audiometry. J Laryngol Otol 127(3): 233-238.

Jaruchinda, P., Thongdeetae, T., Panichkul, S. and Hanchumpol, P. 2005. Prevalence and an analysis of noise--induced hearing loss in army helicopter pilots and aircraft mechanics. J Med Assoc Thai 88 Suppl 3: S232-239.

Kalinec, G.M., Webster, P., Lim, D.J. and Kalinec, F. 2003. A cochlear cell line as an *in vitro* system for drug ototoxicity screening. Audiol Neurootol 8(4): 177-189.

Kaufman, L.R., LeMasters, G.K., Olsen, D.M. and Succop, P. 2005. Effects of concurrent noise and jet fuel exposure on hearing loss. J Occup Environ Med 47(3): 212-218.

Larsen, H.C., Angelborg, C. and Slepecky, N. 1984. Determination of the regional cochlear blood flow in the rat cochlea using non-radioactive microspheres and serially sectioned cochleas. Hear Res 16(2): 127-132.

Lataye, R., Campo, P. and Loquet, G. 2000. Combined effects of noise and styrene exposure on hearing function in the rat. Hear Res 139(1-2): 86-96.

Lawoko-Kerali, G., Milo, M., Davies, D., Halsall, A., Helyer, R., Johnson, C.M., Rivolta, M.N., Tones, M.A. and Holley, M.C. 2004. Ventral otic cell lines as developmental models of auditory epithelial and neural precursors. Dev Dyn 231(4): 801-814.

Lin, B., Ritchie, G.D., Rossi, J., III and Pancrazio, J.J. 2001. Identification of target genes responsive to JP-8 exposure in the rat central nervous system. Toxicol Ind Health 17(5-10): 262-269.

Liu, Y. and Fechter, L.D. 1997. Toluene disrupts outer hair cell morphometry and intracellular calcium homeostasis in cochlear cells of guinea pigs. Toxicol Appl Pharmacol 142(2): 270-277.

Liu, Y., Rao, D. and Fechter, L.D. 1997. Correspondence between middle frequency auditory loss *in vivo* and outer hair cell shortening *in vitro*. Hear Res 112(1-2): 134-140.

Maguin, K., Campo, P. and Parietti-Winkler, C. 2009. Toluene can perturb the neuronal voltage-dependent Ca^{2+} channels involved in the middle-ear reflex. Toxicol Sci 107(2): 473-481.

Pilati, N., Ison, M.J., Barker, M., Mulheran, M., Large, C.H., Forsythe, I.D., Matthias, J. and Hamann, M. 2012. Mechanisms contributing to central excitability changes during hearing loss. Proc Natl Acad Sci USA 109(21): 8292-8297.

Poirier, A.L., Pincemail, J., Van Den, A.P., Lefebvre, P.P. and Malgrange, B. 2010. Oxidative stress in the cochlea: an update. Curr Med Chem 17(30): 3591-3604.

Popelar, J., Groh, D., Pelanova, J., Canlon, B. and Syka, J. 2006. Age-related changes in cochlear and brainstem auditory functions in Fischer 344 rats. Neurobiol Aging 27(3): 490-500.

Rao, D. and Fechter, L.D. 2000. Protective effects of phenyl-N-tert-butylnitrone on the potentiation of noise-induced hearing loss by carbon monoxide. Toxicol Appl Pharmacol 167(2): 125-131.

Raynal, M., Kossowski, M. and Job, A. 2006. Hearing in military pilots: one-time audiometry in pilots of fighters, transports, and helicopters. Aviat Space Environ Med 77(1): 57-61.

Robinson, P.J., Sterner, T.R., Merrill, E.A., Gearhart, J.M. and Mattie, D.R. 2013. Preliminary Mathematical Model for Jet Fuel Exacerbated Noise-Induced Hearing Loss Wright-Patterson AFB, OH: Air Force Research Laboratory, 711th Human Performance Wing, Human Effectiveness Directorate, Bioeffects Division, Molecular Bioeffects Branch. AFRL-RH-WP-TR-2013-0044, ADA582106.

Schaette, R. and Kempter, R. 2012. Computational models of neurophysiological correlates of tinnitus. Front Syst Neurosci 6: 34.

Venet, T., Rumeau, C., Campo, P., Rieger, B., Thomas, A. and Cour, C. 2011. Neuronal circuits involved in the middle-ear acoustic reflex. Toxicol Sci 119(1): 146-155.

Zhou, X., Jen, P.H., Seburn, K.L., Frankel, W.N. and Zheng, Q.Y. 2006. Auditory brainstem responses in 10 inbred strains of mice. Brain Res 1091(1): 16-26.

APPENDIX: PHARMACODYNAMIC MODEL CODE

```
METHOD RK4
STARTTIME = 0
STOPTIME=20
DT = 0.02

FR'=k1*C1+kN*N+kx1*C1*N-kt*GSH*FR-k2*FR*PUFA; Free radical kinetics
init FR=0
k1=0.5 ; chemical-induced FR formation
C1=1.2 ; chemical concentration
kN=1 ; Noise-induced FR formation
N0=1 ; noise level
N= step(N0, 4)+step(-N0,6) ; Burst of noise
kx1=0 ; cross-term between noise and chemical
kt=1 ; FR degradation

GSH'=G+kg*GSSG-kt*GSH*FR-ktp*PUFAR*GSH-ktpr*PPUFAR*GSH ; Glutathione (or
generic anti-oxidant)  kinetics
GSSG'=kt*GSH*FR-kg*GSSG+ktp*PUFAR*GSH+ktpr*PPUFAR*GSH ; inactivated form
ktp=1 ; removal of PUFA radical
ktpr=1 ; removal of peroxyl PUFA radical
G=0 ; glutathione synthesis
init GSH=1.5
init GSSG=0.5
kg=1 ; rGSH recycling

limit FR>=0
limit GSH >=0
limit GSSG >=0

R=GSH/GSSG ; active/inactive GSH ratio

A'=-kd*FR+kr*I - kdr*PUFAR - kdpr*PPUFAR ; Active hair cells, kr is repair
I'=kd*FR-kr*I -kp*I + kdr*PUFAR + kdpr*PPUFAR; Inactive hair cells
P'=kp*I ; permanently inactive (dead) hair cells
init P = 0
kdr=1 ; inactivation of hair cells by PUFAR
kdpr=1 ; inactivation of hair cells by PPUFAR
kd=0.1 ; inactivation of hair cells by FR
kr=0.3 ; repair of inactivated hair cells
kp=0.1 ; death of inactivated hair cells
init A=1
init I=0
limit A>=0
limit I >=0
```

```
limit A<=1
limit I<=1

;-----------------------------------

PUFAR'=k2*FR*PUFA-k3*O2*PUFAR+k4*PPUFAR*PUFA - ktp*PUFAR*GSH ; PUFA
radical kinetics
PUFA=1 ;  polyunsaturated fatty acid in membrane (assumed constant)
init PUFAR=0
k2=1 ; conversion of PUFA to PUFA radical by FR

PPUFAR'=k3*O2*PUFAR-k4*PPUFAR*PUFA - ktpr*PPUFAR*GSH ; PPUFA kinetics
O2=1 ; oxygen concentration assumed constant (not rate limiting)
init PPUFAR = 0
k3=1 ; peroxyl PUFA formation rate constant
k4=1 ; lipid peroxide formation rate constant

MDA'=k3*PPUFAR*PUFA
init MDA=0
```

LIST OF ACRONYMS

ABR	auditory brainstem response
ADP	adenosine diphosphate
AFB	Air Force Base
AFOSR	Air Force Office of Scientific Research
AFRL	Air Force Research Laboratory
AKAP	kinase A-associated protein
ANOVA	analysis of variance
ATP	adenosine triphosphate
ATR	DNA damage sensor kinase
CANS	central auditory nervous system
CAPD	central auditory processing dysfunctions
DMEM	Dulbecco's modified Eagle's medium
DMSO	dimethyl sulfoxide
DPOAE	distortion product otoacoustic emissions
DTIC	Defense Technical Information Center
FBS	fetal bovine serum
FR	free radical
$GABA_AR$	gamma-aminobutyric acid A receptor
GAT-3	GABA transporter 3
GO	gene ontology
GSH	glutathione
GSSG	glutathione disulfide
HEI-OC1	House Ear Institute Organ of Corti 1
HJF	Henry M. Jackson Foundation for the Advancement of Military Medicine
ID	Identification
ITPR2	inositol trisphosphate receptor
KEGG	Kyoto Encyclopedia of Genes and Genomes
LC-MS/MS	liquid chromatography-tandem mass spectrometry
LP	lipid peroxides
LRIR	Laboratory Research Initiation Request
LTQ	linear trap quadripole
MAP1	microtubule-associated protein
MDA	malondialdehyde
MER	middle ear reflex
MTS	3-(4,5-dimethylthiazol-2-yl)-5-(3-carboxymethoxyphenyl)-2-(4-sulfophenyl)-2H-tetrazolium
NIHL	noise induced hearing loss
NIOSH	National Institute for Occupational Safety and Health
OSHA	Occupational Safety and Health Administration
PBPK	physiologically-based pharmacokinetic
PBS	phosphate buffered saline
PC	partition coefficient
PD	pharmacodynamic
PEL	permissible exposure limit

PPUFAR	peroxy polyunsaturated fatty acid radicals
PUFA	polyunsaturated fatty acids
PUFAR	polyunsaturated fatty acid radicals
REL	recommended exposure limit
SPTLC3	palmitoyl transferase
TBARS	thiobarbituric acid reactive substance
TCEP	tris (2-carboxylethyl) phosphine hydrochloride
TEAB	triethyl ammonium bicarbonate
TMT	tandem mass tags
UCLA	University of California Los Angeles
VDCC	voltage-dependent calcium channels